Studies and Investigations related to the Development of a Potato-Rock Separator

by

Jacob Melvin Boby Sagayaraj

Submitted in partial fulfilment of the requirements
for the degree of Master of Applied Science

at

Dalhousie University
Halifax, Nova Scotia
July 2019

I dedicate this thesis to my parents, teachers and friends who have constantly supported and motivated me during my studies.

Table of Contents

List of Tables

List of Figures

List of Symbols Used

μ	Eddy Viscosity
k	Turbulent Kinetic Energy
ε	Rate of dissipation of turbulent kinetic energy
ρ	Mass density
Q	Heat Transfer rate
U_{mf}	Minimum fluidization velocity
U_{th}	Transport gas velocity
U_g	Superficial gas velocity
U_{mb}	Minimum bubbling velocity
U_{ms}	Minimum slugging velocity
U_c	Critical velocity
D	Fixed bed diameter
D_b	Bubble diameter

Abstract

This thesis reports work on a two-part research towards the development of an improved Potato-rock separator. The work was carried out in the industrial setting of a factory named Allan Equipment (AE) at Prince Edward Island. First part of the work involved improvement of a 'wave bed' based separator unit that was developed and built by this company. The second part of the work involved development of a new type of potato-rock separator using fluidized bed principles.

In part one, we used fluid dynamics simulation to understand why the existing design of AE gave poor performance and discovered that it is due to non-uniform air flow distribution caused by their current duct layout and air plenum design. CFD simulation suggested change in fan arrangement, which was done by AE in their full-scale commercial unit. Our experiments on this modified unit confirmed the more uniform flow distribution CFD simulation predicted. Since this improvement was not adequate for AE, we used CFD simulation to further evaluate other options. CFD simulation predicted that addition of a perforated plate in plenum chamber could result in more uniform air distribution. AE implemented this change. Our experiment on this unit confirmed the improvements predicted by CFD. AE wanted further modification to have certain velocity distribution above their wave bed. This part of the work was done without simulation but by building plates of different hole size and arrangements. Experiments on these different designs showed the best combination of hole and arrangement to best meet the requirement of AE.

In the second part we designed and built a bench scale fluidized bed of sand to explore if bubbling fluidized bed can be used to separate mixture of potato and rocks which are order of magnitude larger than the bed particles. After measuring pressure drop characteristics of the fluidized bed system, we dropped mixture of potato and rocks. We fluidized the bed at different fluidizing velocities and found that such over sized particles can be separated, but the degree of separation is a function of fluidization velocities. We measured the segregation of the particles along the depth of the bed with change in fluidizing velocity. Finally, we found the optimum velocity for these particles. Thus, this work established the potential of development of new type of potato-rock separator based on fluidized bed principles.

Acknowledgements

I extend my sincere thanks and gratitude to my supervisor Dr. Prabir Basu for his invaluable guidance and support. I am eternally grateful to him for providing me with an opportunity to work under supervision. His constant advice, motivation and feedback have helped me greatly. I would like to thank Dr. Bishnu Acharya for his timely guidance and making me feel at home during my stay in PEI. My sincerest thanks extent to Mr. Akash Kulshreshtha, who has been my mentor throughout this research and has constantly motivated and guided me to achieve deadlines. I thank Mr. Lyle Gauthier, Mr. Danie and the staff of Allan Equipment for their support and help in carrying out my research. I would also like to thank members of my guiding committee, Dr. Ismet Ugursal and Dr. Sophia He for their support and guidance in my work.

Finally, I would like to thank NSERC for providing some funds for this project and all faculty and staff of the Mechanical engineering department for providing me with inspiration and the best academic experience.

Chapter 1: INTRODUCTION

This chapter discusses the objective of research and organization of the thesis

1.1 OBJECTIVES AND MOTIVATION OF THESIS

The motive behind this thesis is arriving at a solution for effective separation of binary particles (potato and rocks) by employing the principle of buoyancy separation. The research starts out with the initial stages of experimentation. The air duct system of the harvester under current use showed poor efficiency of separation. So, its duct design was subjected to experiments. Uniform air flow through the grate above the air duct's exit was to be achieved. The first half of the research involved study of the fluid flow through it and comparison of measured data with those predicted by Computational Fluid Dynamic simulation. A relation between the experimental and theoretical result was to be achieved. Once the CFD results are calibrated through this verification, CFD simulation can be used to carry out necessary hardware changes to the design of the system. This could avoid unnecessary use of manpower and resources.

The above exercise did not attempt to make any change in the current design of buoyancy separation where potato and rocks are selectively levitated by air flow through the air box grid. The second half of the research involved a different means of separation. It employed fluidization principle to separate two types of heavier and lighter particles. It involved the design of a fluidized bed to study the density and size behaviour of the binary particle in a fluidized medium. The characteristics of the particles (Potato and Rocks) under the influence of varied fluidization velocities were studied, to predict a higher separation efficiency.

1.2 THESIS ORGANIZATION

Chapter 2 and 3 of this thesis explores the design aspects of the air duct system under study and the experimental setup of the system. The different layouts used and the initial design leading up to the final design are shown with figures of the air duct system of the harvester under study. The experimental setup for the computational fluid dynamics test to be run. Proving the boundary conditions based on the experimental results obtained from the initial stages of testing is done in this chapter. The pre-processing and post-processing experimental setup is discussed in this chapter.

Chapter section 2.3 includes the experimental results and discussion of the thesis. The experimentally obtained results of the air duct system is compared with the CFD results and a correlation between the two is obtained to assure accuracy in CFD results.

Chapter 3 introduces the design of sand fluidized bed and also presents a review on the different fluidization regimes. The design of the sand chamber is described. Experimental setup for the fluidized bed is discussed in this chapter, showing the density characteristics of the potatoes and rocks (Objects under study). The results of the experiments of the sand fluidized bed are discussed.

Chapter 4 aims to conclude the results of the thesis and suggestions for future work to the current research is given.

Chapter 2: IMPROVEMENT OF EXISTING DESIGN

2.1 BACKGROUND

2.1.1 History of harvesters

Potato harvesting is a major agricultural activity of Prince Edward Island, where the need for faster yet efficient means of harvesting is of growing importance. Potato, the 4th highest cultivated commodity in the world, is harvested from the field by large machineries. The mechanical means of digging potato from the ground picks up from the field lots of undesired entities such as rocks, vines and dirt along with the potato. Separation of rocks from harvested potato is thus a critical step in this production cycle.

Over generations the means of harvesting have changed drastically, both in terms of cost and the time spent on harvesting. Manual means of harvesting has been around for centuries, which involved more manpower and time consumption. Picking/digging up of the potatoes were later replaced with a potato spinner which was connected to a tractor. The potato spinner was made up of a metal spindles that dug up the soil and pushed the potatoes outside and on to the sides to be picked up. With a growing population and increased cultivation of these spuds, the need for more advanced machinery rose, and this led to the development of harvesters. The harvesters are not limited to the use for extraction of potatoes alone, they could be used for other cultivations if the need be.

In the food industry sector, the food products are considered fit for use only when the extracted product delivered to the customer is of good physical quality and void of damage. When the potatoes are extracted from the field, rocks also get extracted from the soil in the harvesting zone. When the potatoes and rocks travel together in a conveyor belt, the abrasion of the rocks along with the potato can cause physical damage to the potatoes. The damage to these potatoes can be limited to a greater extent by separating the rocks and the potatoes at the initial stages of harvesting. Selective picking of these potatoes and rocks would be very tedious and hence mechanisms employing fluid mechanical mediums for separation of these binary particles have evolved and adapted over the past few years.

Figure 1. Potato Spinner [1]

The modern age harvesters have single and multiple rows for digging up the harvest and conveying them to the load trucks. Although de-stoning techniques which involve the removal of rocks from the soil are being employed in a few places in the world, they have not garnered the level of standard use in all cultivating potato farms, as these are non-economical. The manufacturers of these harvesters comply with the needs of the cultivators and in most cases the potatoes are cultivated in rock containing fields.

The harvest is done in three stages 1) Sieving, 2) Separating and 3) Conveying. The sieving stage involves the digging up of the spuds and rocks from the soil. The second stage which is the separation stage varies from place to place and is entirely based on design and adopted technology. Techniques such vibrating tables, swing agitators and air separation have been used effectively for separation of the binary particles. The air separation technology provides with the highest efficiency in separation. In this system the vines that come along the conveyor also get blown out from the separation grate making the entire system more efficient while serving multiple purpose.

The aim behind harvesting of these potatoes is to achieve the complete recovery of crops, minimum damage and a healthy clean sample. Separation technologies in the

present market are based on their use and most of the mechanical systems are patented. The buoyancy technique is being widely used because of its relatively low initial cost. Here, a directional air flow moves away the potatoes and rocks while they are lifted by a fluid medium. The technique of using sensors that are capable of identifying the rocks and potatoes, is another patented technology in the market, but is not widely used because of the high maintenance and initial cost. Vigorous agitators make use of dynamic characteristics of the potatoes and rocks to achieve separation, because of the varied physical properties of the rocks and the potatoes. This technique can cause much damage to the spuds and is hence not widely used.

The currently active and widely known harvester manufacturers, *Spudnik* makes use of the buoyancy separation machine which incorporates mechanical and electrical means to achieve separation of the potatoes [2]. A directional stream of air is passed through a grate onto which the potatoes fall on top of a vibrating surface. The forced air prevents the potatoes from mixing with the rock removal section and the vibration helps in the movement of these two binary particles. The removal of the rocks is by means of finger gates that only allow passage for the rocks but not the potatoes. The design is currently protected by patents [3].

Air suction potato harvesting techniques also found in patents and are being used by some farm equipment worldwide [4]. This technique employs the suction of air, which gathers vines and small stones, leaving behind the potatoes which then travel to collecting bins. The suction technique does not separate large rocks from the mixture of particles. Centrifugal separation also could be used in separation systems, but the rotating action can cause damage to the potatoes and making it unfit for use. A similar version of this can be found in the manufactures Milestone [5] and Harrison [6]. In addition to the such electrical and mechanical systems some researches have been conducted on fluidized bed to achieve separation of binary particles in a sand medium [7]. These systems have a very high efficiency of separation although the maintenance of such systems would be very difficult. Extended research is required for implementing such a complex design.

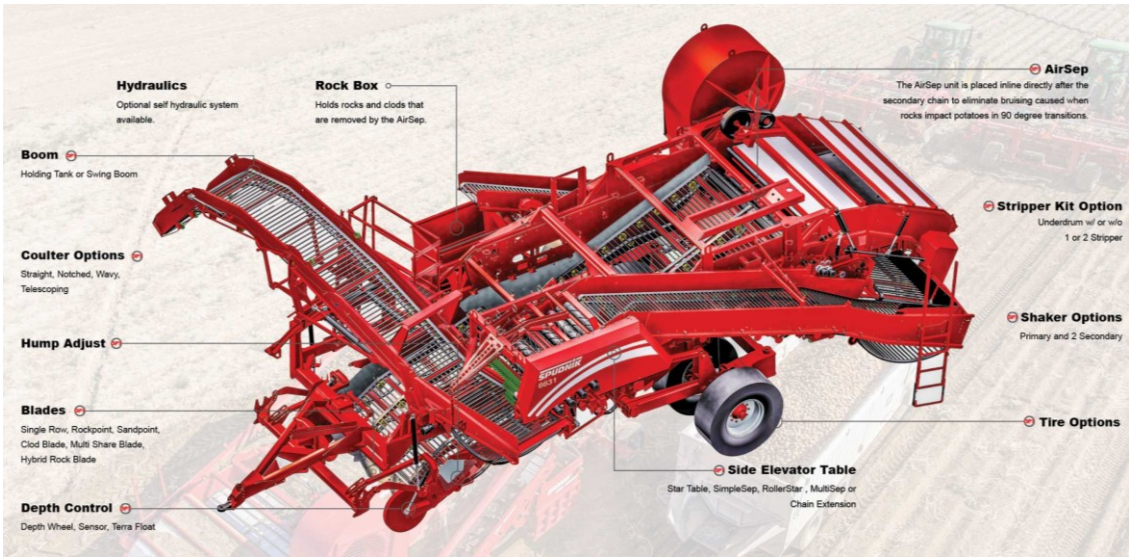

Figure 2. Spudnik's 3 Row harvester (Image taken from the Spudnik website) [2]

2.1.2 Evolution of CFD

Since the advent of computers, computational fluid dynamics (CFD) has been playing an integral part analysis of fluid flow. It is helping researchers achieve what they desire in a very short period of time. The growth of CFD over the past few decades has been enormous, and its user interface has increased dramatically [8]. Its capacity to solve mathematical equations with ease has made CFD an essential tool in the scientific world. Complex processes involving heat transfer, mass transfer and momentum transfer are mathematically modelled using the simulation tool of CFD [9].

Simulation of real life flow is one of the key areas in which CFD play a very important part. The modeling for turbulence irrespective of the physical geometrical size can be done easily [10]. Scaling of the model helps arrive at a solution and also greatly reduces development cost. Aerodynamic simulations, with the help of a greater computing power has helped the aerospace sector greatly wherein the lift and drag tests are initially done with just simulations.

2.2: DESIGN OF ROCK-POTATO SEPARATOR

Harvesting mechanisms have greatly changed over time, with automated harvesting replacing manual means. The rock separator is designed in such a way that the feed is continuous and in large throughput. The rock separator works with the assistance of air that is supplied with the help of a radial fan. In the present research, the air duct in the harvester was modified on the basis of critical analysis of experimental data obtained.

2.2.1 Initial design of the binary particle separator

The preliminary design of the separator, by Allan Equipment Manufacturing Ltd. is shown in Figure 3. The design makes use of an air distribution system and a special grate aiding in the separation of particles. The fan was originally located at the top of the harvester and was connected to a duct that made two 90^{O} bends and ended in the air plenum (Figure 4). The fan was later brought right at the inlet section to avoid 90° turns and thereby provide better uniformity in air supply. One of the main reasons to house the fan on the top of the harvester, was for the harvester to operate in the field. The change of the fan position from the top to the inlet is in situations where the harvester would operate off-site. It may, however, be noted that placing the fan at a lower position can cause imbalance to the harvester and make its operation in the field difficult

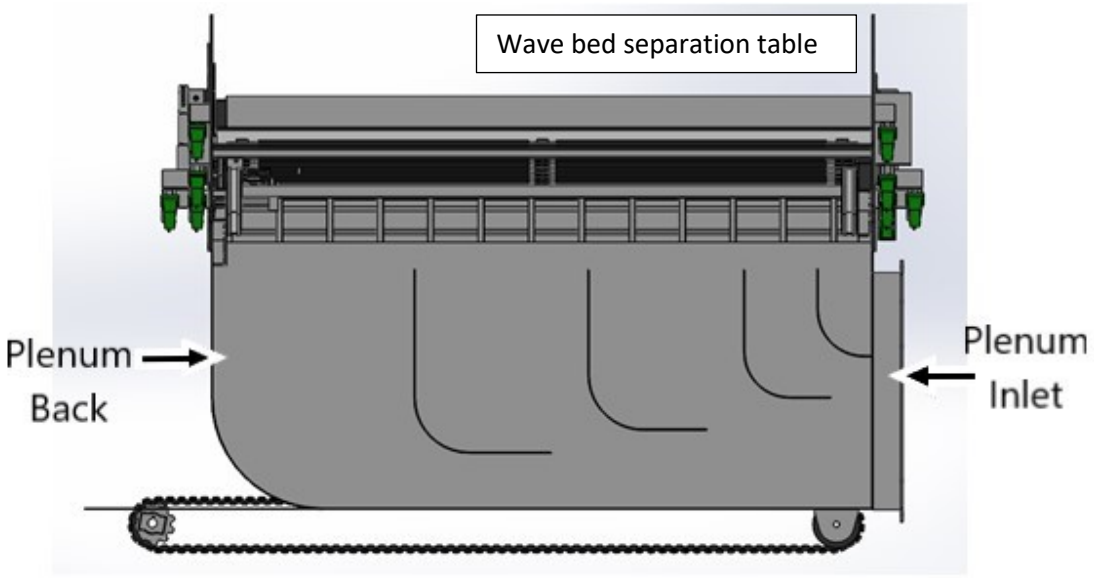

Figure 3. Design of the Potato-Rock separator – Front View

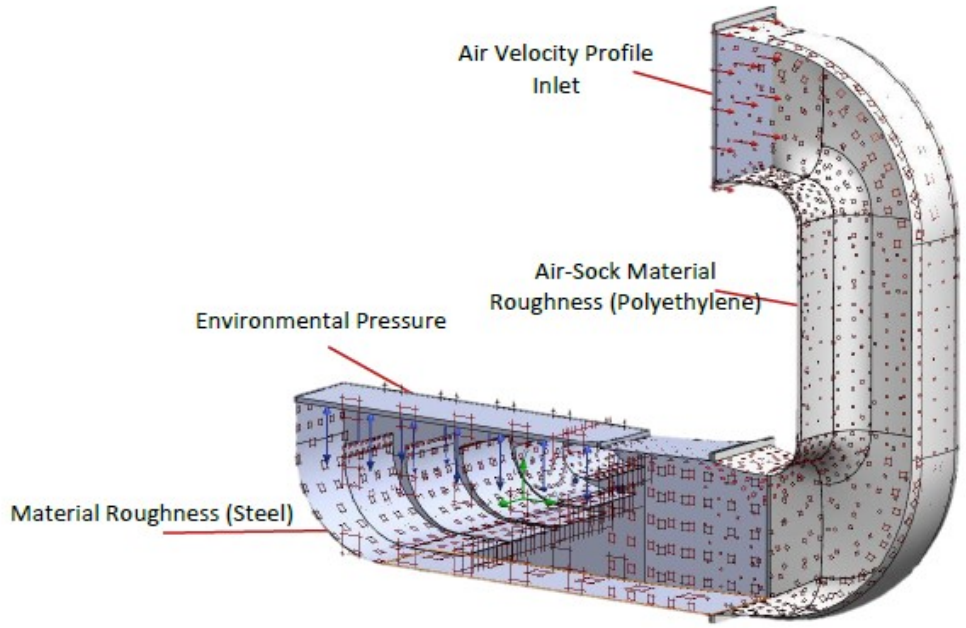

Figure 4. A 3-D image of the original design of the air plenum connected to the fan by means of an air sock

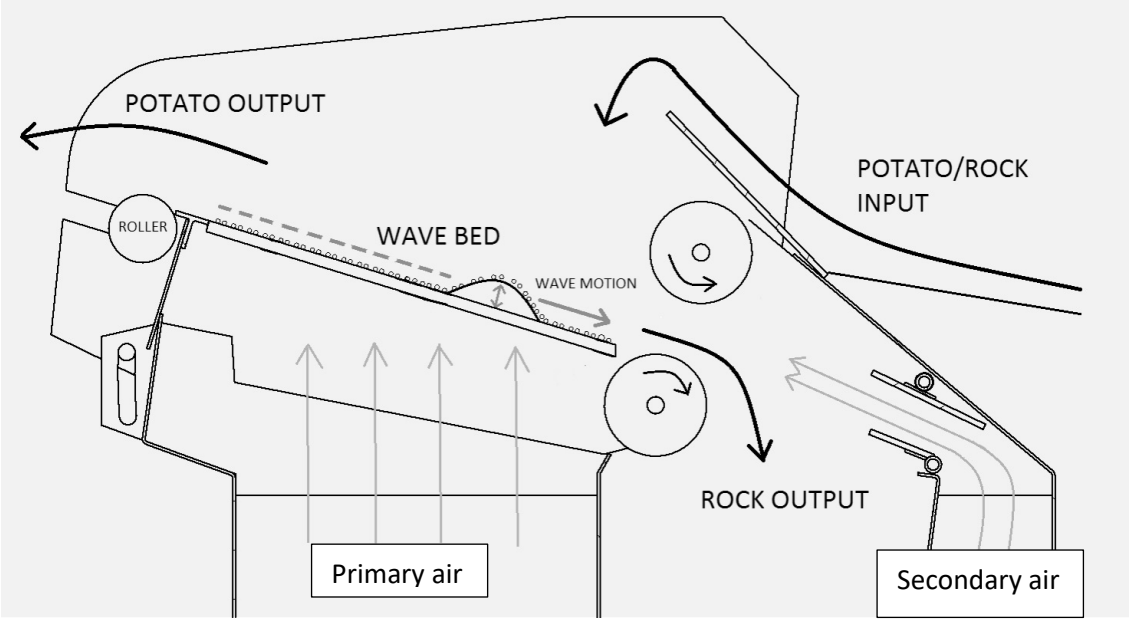

Figure 5. Side view from the plenum inlet showing the wave bed separation table and entry of secondary air to move potato off the table

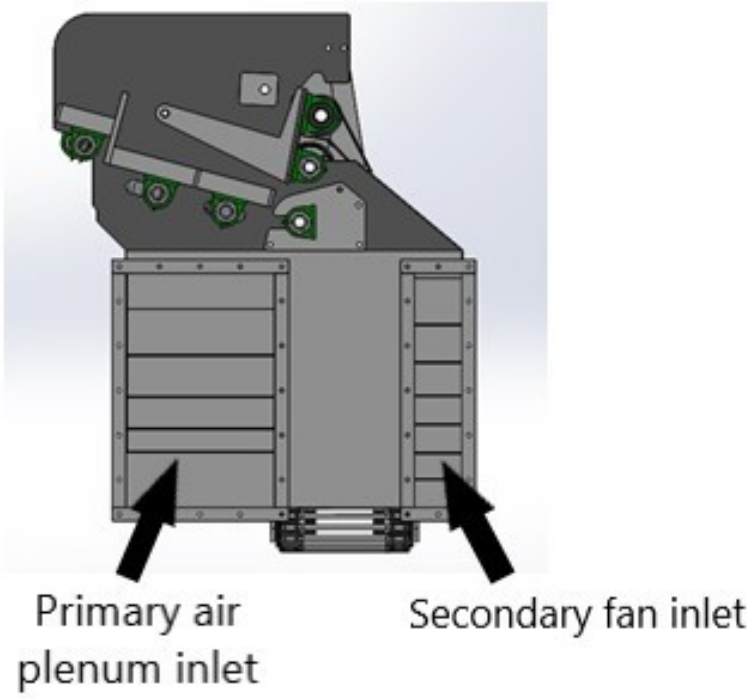

Figure 6. Side view from the plenum inlet of the air duct system

2.2.1.1 Wave-Bed and Air Distribution System

The fan, initially placed above the harvester, used in this system is a radial fan of 17,200 cubic feet per minute (8.11 m^3/s) discharge and static pressure 228 mm water gauge (wg). This fan, manufactured by IAP Inc, provides air to the wave bed. The fan is mounted at the inlet of the duct system and is capable of functioning at different speeds with the help of Programmable Logic Controller and a Variable Frequency Drive. Such fans are currently used in most harvesting machines made at Allan Equipment Manufacturing Ltd. Its volumetric flow capacity is adequate to supply enough air to levitate potatoes above the wave bed. The potatoes are levitated by air, but the rocks remain at the bottom due to their higher density. The wave or oscillating action of the belt facilitates the separation of the rock. It is done with the help of pinch rollers (Figure 5). Present research was carried out at around 80 % fan load, which is the maximum operating load of the harvester in field.

In addition to this main fan, there is also a secondary (back) fan which is connected to a rear duct that sends air through the duct and into the pinch rollers present at the rock removal section. This secondary fan makes sure that the potatoes do not come out of the pinch rollers when the separation takes place (Figure 6).

The Wave-bed is a unique mechanism used at Allan Equipment Manufacturing Ltd. It imparts a wave motion that can be operated at different speeds. The belt is made up of steel rods coated with rubber that are thinly spaced. The portion below the belt consists of disks attached to two individual rods which move along an elliptical track and come in contact with the wave bed along its width. This produces the wave action on the bed. The wave bed design is shown in Figure 7.

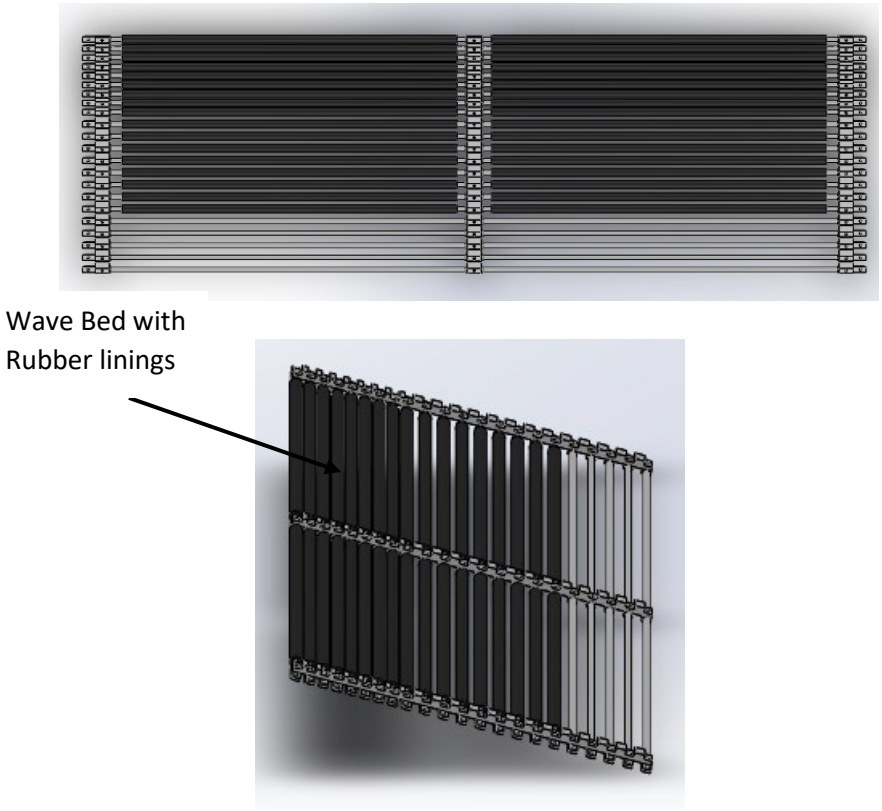

Figure 7. Plan view of the Wave bed that sits on top of the air plenum. This figure also shows equally spaced rollers with rubber coatings of different thickness resulting in different opening for air flow

2.2.2 Problems faced in the preliminary design

In the initial design, difficulty in separation was noticed because the velocity of air above the wave bed was not uniform. This lack of uniformity could be attributed to the design of the baffles inside the wave bed. The unevenness of the air velocity resulted in the piling up of the potatoes on one side of the air plenum, leading to inefficient separation.

2.2.3 Work strategy employed

CFD simulation was used to reduce the development effort and cost by avoiding multiple changes in hardware. We ran simulation 1 to predict the velocity distribution

of the air above the wave bed with the existing configuration of duct layout. It showed very high air velocity towards plenum-back end of the air duct and very little in the plenum inlet edge of the air box. Although we did not conduct any experiment (Allan equipment was under time constraints), this observation qualitatively agreed with visual observation of the industry and explained the reason for the inefficient separation. Based on simulation 1, we advised Allan Equipment to relocate the fan.

We ran a second simulation to check if the non-uniformity could be improved by relocating the fan in line with plenum inlet (Figure 29). Simulation results showed good improvement (Figure 31).

To verify the theoretically predicted results of simulation 2, we performed an experiment and compared results (Figure 32). A reasonably good agreement between the simulation and experimental data raised our confidence of the simulation.

We then noted that to flatten the dip in velocity distribution (Figure 32), we could provide additional resistance as is done in the design of fluidized beds. After which we decided to install a perforated plate below the wave bed (Figure 7). Before proceeding with this, we ran simulation #3 and observed it could make the flow uniform.

Based on simulation #3 we advised Allan Equipment to install the perforated plate of uniform hole distribution. The installed Perforated plate is shown in (Figure 12). We performed experiments to verify the simulation results and found good agreement with predicted values as shown in Figure 34. Although this achieved the desired goal of uniform velocity distribution, the overall maximum discharge of the centrifugal fan reduced due to increased flow resistance caused by the perforated plate.

Additionally, Allan Equipment wanted more airflow rate on the right edge of the plenum. For that reason, we first tried to run simulations with different holes in different areas of the perforated plate. This made CFD simulations extremely complex. Because of the time constraints of our industry partner, we had to discontinue simulation-based development and adopted experimental based industrial approach.

We prepared perforated plates of different fractional opening in different sections with holes of different sizes. Again, due to time limitations we could not carry systematic investigation of the effect of different combination of holes and fractional openings. Instead we relied on the many years of industrial air box designs of my supervisor. We

prepared several designs of perforated plates and have Allan equipment make them. We tested these perforated plates for the resulting flow distribution and found out that Layout IV gave the best design results (Figure 17)

2.2.4 Computational fluid dynamics analysis

To analyze the fluid flow around a domain or inside it, one can use computational fluid dynamics. The simulation can be done with the help of different commercial software. In the present research, we use COMSOL software for carrying out CFD analysis for the given model. CFD allows the modeler to predict the velocity, pressure or temperature at any point in the modelled system.

CFD Modelling is generally a 3 step procedure, the first being pre-processing which involves the establishment of the model/geometry, definition of boundaries and physics characteristics. The definition of boundaries specifies the wall, the fluid and the solid in contact with the fluid. In the second step, a CFD model divides the geometry into a set of mesh. The meshing options are available for both 2D and 3D flow geometries. After the meshing of the geometry, the post-processing stage is carried out, which involves solution of the flow field. The study has different solvers serving different purposes, including steady and time-dependant analysis.

The boundary conditions are the most important parameters that define the flow and as such it needs to be properly assigned to get an accurate result. The fluid flow problem can be solved with various models rendering different purposes. In any case, results of a CFD analysis is validated by confirming them with the experimentally obtained data.

2.2.4.1 Turbulence Models

Computational fluid dynamics (CFD) is a numerical analysis which uses governing fluid flow equations to solve fluid flow through or around a domain. They are generally partial differential equations that become algebraic expressions when they are discretized around a mesh. These equations are solved by either finite difference method/finite volume method algorithms. Computational cost, a term that would be used frequently in this chapter, is the computational effort that is required by a computer which is related to the time of computing a given model. It comes from the early days of computation when computer operation was expensive, and users had to wait for an extended period of time in using of the machine to arrive at a result.

The most common technique to analyse turbulent flow in CFD is by using the Reynolds Averaged Navier-Stokes (RANS) equation that models the flow by utilizing Reynolds decomposition in which an instantaneous flow quantity is broken into a time dependent flow and time averaged quantity. The turbulence flow properties are difficult to get but are necessary to produce the time averaged solution based on approximations for the fluid flow. There are some methods such as the Large eddy simulation (LES), Direct Numerical Solution (DNS) and Detached Eddy Simulation (DES) [11]. The RANS model has the lowest computational cost compared to other methods. Although the errors are less in other models, they have a higher computational cost. The LES model calculates the intermediate-scale motions, large scale motions as well as the mean scale flow. The DES method splits the flow domain into two layers which makes use of both the LES model and RANS model. The DES has lesser computational cost than the LES model. The DNS method is the most accurate and commonly used method for solving turbulent fluid flows, as it directly solves Navier-Stokes equation for the entire mesh. The DNS has a high computational cost but is heavily used when solving CFD involving simple flow domains [12].

When choosing the turbulence model for solving a CFD, a compromise on the computational cost can cause inaccuracies to a certain extent. The hardware capabilities of the computing device are also to be considered while setting up the solver for analysis.

2.2.4.2 Pre-Processing

The initial stage of analysis involves the development of the duct geometry. In the research carried out for this thesis, we draw the duct in Solid-Works and then import the 3D geometry from this software, which could have alternatively been modelled directly in COMSOL. The imported geometry is the first domain and a second domain are created so as to fill up the cavity inside, to specify it as an air domain. Once the geometry is created, an assembly is formed. The material characteristics are pre-defined, the walls are steel, and the fluid domain is air. When the perforated plate is introduced into the geometry, we add an extra material to this. Over the period of this research constant changes to the geometry was made so as to account for the changes made to the experimental setup.

The introduction of a perforated plate drastically increased the complexity of fluid flow and therefore the computational cost, as it was a complex geometry housing many perforations. Perforation size was an important parameter in the current simulation as a higher computational cost was required to produce an accurate result.

2.2.4.3 Modelling Physics and k-ε Turbulence Model

After importing and modelling of the geometry, the geometry of the flow field is defined. The COMSOL application allows us to define the physics of the geometry through boundaries, edges and domains. The flow through the air duct can be numerically solved using many models in the software. In this thesis we make use of the Reynolds Averaged Navier-Stokes equation. The RANS model is the most widely used solver and it also has a lesser computational time/cost. Although an LES/DNS model would provide a more accurate result, the need for lower computational cost was of prime importance because of the limited hardware capabilities [13], as time constraints to provide results was also of prime importance. Since air is supplied by means of a centrifugal fan, a rotational flow can be evident and hence turbulent flow is assumed. The k-ε model and the RANS equations are coupled together to solve for the air flow problem. The equations involving the conservation of momentum, mass and energy are replaced by the mean and fluctuating quantities. The time averaging equations are transformed into the RANS equations after performing these substitutions and are as follows [14] [15].

Conservation of Mass

The conservation of mass in x, y and z co-ordinates is given by the equation [15]

$$\frac{\partial(\rho\bar{u})}{\partial x}+\frac{\partial(\rho\bar{v})}{\partial y}+\frac{\partial(\rho\bar{w})}{\partial z}=0 \qquad \text{Eqn. [1]}$$

Conservation of Momentum

x-axis momentum [15]

$$\frac{\partial}{\partial t}(\rho\bar{u})+\frac{\partial}{\partial x}(\rho\overline{uu})+\frac{\partial}{\partial y}(\rho\overline{vu})+\frac{\partial}{\partial z}(\rho\overline{wu})=$$

$$-\frac{\partial\bar{P}}{\partial x}+(\mu+\mu_t)(\frac{\partial^2\bar{u}}{\partial x^2}+\frac{\partial^2\bar{u}}{\partial y^2}+\frac{\partial^2\bar{u}}{\partial z^2}) \qquad \text{Eqn. [2]}$$

y-axis momentum [15]

$$\frac{\partial}{\partial t}(\rho\bar{v}) + \frac{\partial}{\partial x}(\rho\overline{uv}) + \frac{\partial}{\partial y}(\rho\overline{vv}) + \frac{\partial}{\partial z}(\rho\overline{wv}) =$$

$$-\frac{\partial \bar{P}}{\partial y} + (\mu + \mu_t)\left(\frac{\partial^2 \bar{w}}{\partial x^2} + \frac{\partial^2 \bar{w}}{\partial y^2} + \frac{\partial^2 \bar{w}}{\partial z^2}\right) - \rho g \beta (T_\infty - T) \qquad \text{Eqn. [3]}$$

z-axis momentum [15]

$$\frac{\partial}{\partial t}(\rho\bar{w}) + \frac{\partial}{\partial x}(\rho\overline{uw}) + \frac{\partial}{\partial y}(\rho\bar{w}) + \frac{\partial}{\partial z}(\rho\overline{ww}) =$$

$$-\frac{\partial \bar{P}}{\partial x} + (\mu + \mu_t)\left(\frac{\partial^2 \bar{w}}{\partial x^2} + \frac{\partial^2 \bar{w}}{\partial y^2} + \frac{\partial^2 \bar{w}}{\partial z^2}\right) \qquad \text{Eqn. [4]}$$

Conservation of Energy

The conservation of energy equation is as follows [15]:

$$\frac{\partial}{\partial t}\left(\rho C_p \bar{T}\right) + \frac{\partial}{\partial x}\left(\rho C_p \bar{T}\bar{u}\right) + \frac{\partial}{\partial y}\left(\rho C_p \bar{T}\bar{v}\right) + \frac{\partial}{\partial z}\left(\rho C_p \bar{T}\bar{w}\right)$$

$$= Q + k\left(\frac{\partial^2 \bar{T}}{\partial x^2} + \frac{\partial^2 \bar{T}}{\partial y^2} + \frac{\partial^2 \bar{T}}{\partial z^2}\right) \qquad \text{Eqn. [5]}$$

The **k-ε** model determines the eddy viscosity (*μ)* based on the turbulent kinetic energy (*k),* the energy per unit mass for the eddies and the turbulent dissipation rate kinetic energy (*ε).* The turbulent kinetic energy is achieved as a result of the fluid shear or other external forces. The initial boundary conditions and the turbulence condition have to be specified for the k-ε model. Parameters such as the turbulent intensity (0.5 %) and turbulent length scale are determined with the help of the turbulent kinetic energy, in the software [16].

There are two options in the **k-ε**; the segregated solver or the coupled flow solver. The segregated flow solver has a lesser computational time than the coupled flow solver and is used in this thesis.

Tests were carried out by placing a pitot tube connected to a manometer to determine the outlet velocity of the blower/centrifugal fan. The average of 3 points was taken for this case, to obtain the velocity of air coming out of the fan. The outlet fan velocity that was determined, is the inlet velocity of the air duct and is defined in our geometry. The average velocity over all the measured points was 33 m/s. The inlet and the outlet conditions are specified for the geometry, mentioned below.

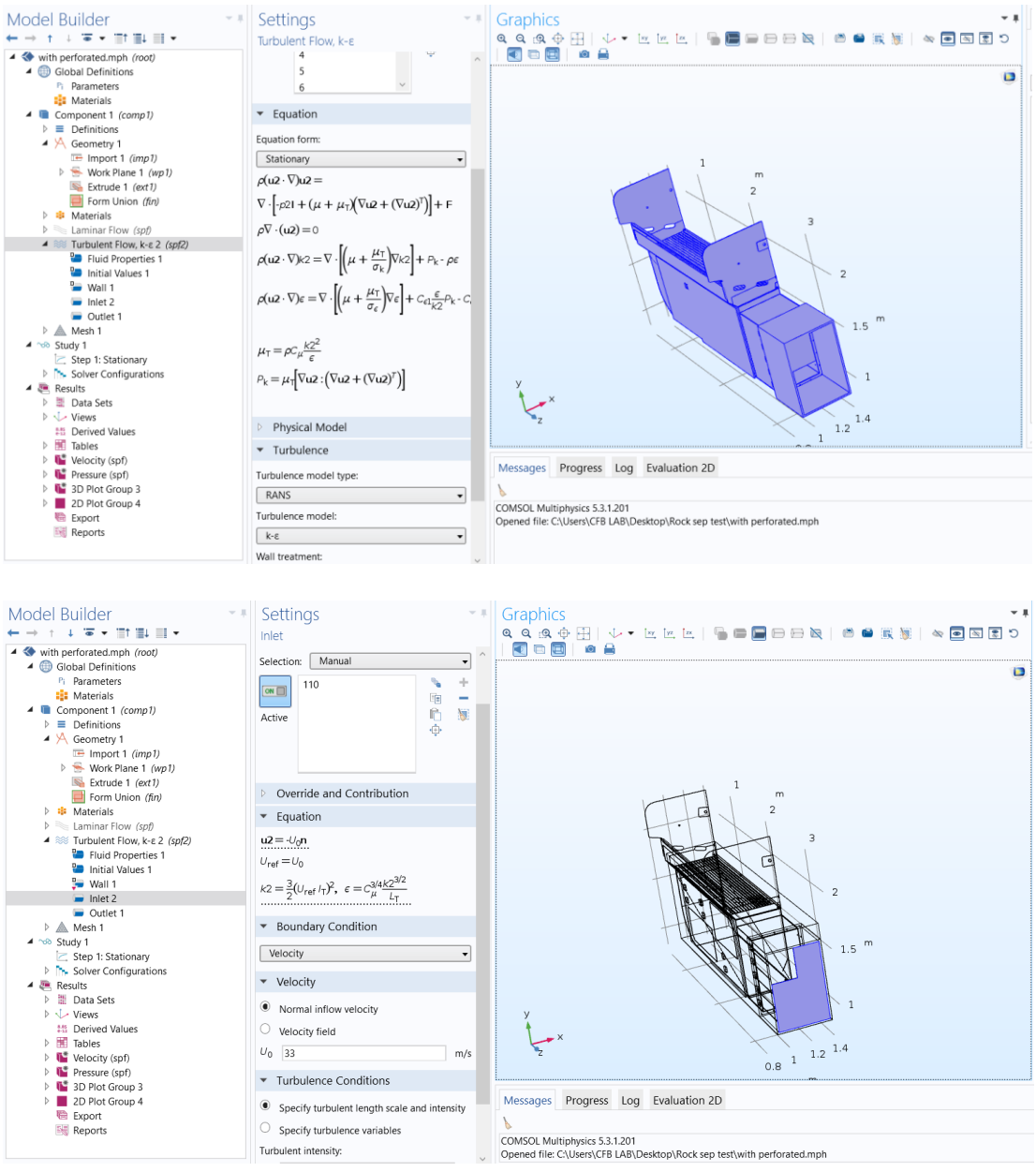

Figure 8. COMSOL snippets with the turbulent model and the boundary conditions specified

The fluid properties and assumptions made in the model are as follows

- Three-Dimensional

- Steady state
- Fluid Medium – Air
- Density of air = 1.204 kg/m^3
- No slip wall condition
- Specific Heat of air = 1006.43 J/kg-K
- Viscosity of air = 1.82 x 10^{-5} kg/m-s
- Atmospheric outlet pressure
- Inlet velocity = 33 m/s
- Gravity acting in the negative y direction at 9.81 m/s^2
- Stationary study

2.2.4.4 Development of mesh

Many models when performing CFD requires manual meshing, which is time consuming but efficient in many ways. A bigger mesh size would reduce the computational cost, but the end result would be inaccurate. The manual meshing strategy is often employed in industries and other sectors to reduce the computational time. In manual meshing, the complex parts are meshed in finer sizes, whereas in parts of the geometry that are non-important or insignificant, a coarser mesh is used. Regions in the geometry that have the physics defined are usually regions that need to have a finer sized mesh. Although the definition of the models affects the computational cost, an efficient mesh can reduce the computational cost at a higher percentage [17]. There are many meshing software that can be used to create a mesh, some of them include Hypermesh, Materialize 3-matic and +SCANFE [16]. These software can be used to define a mesh and can be imported into the CFD solver. In this thesis we use the inbuilt mesh in COMSOL, that has a physics controlled mesh, which automatically generates a mesh (Figure 9). Manual meshing was also employed at times to reduce the computational cost.

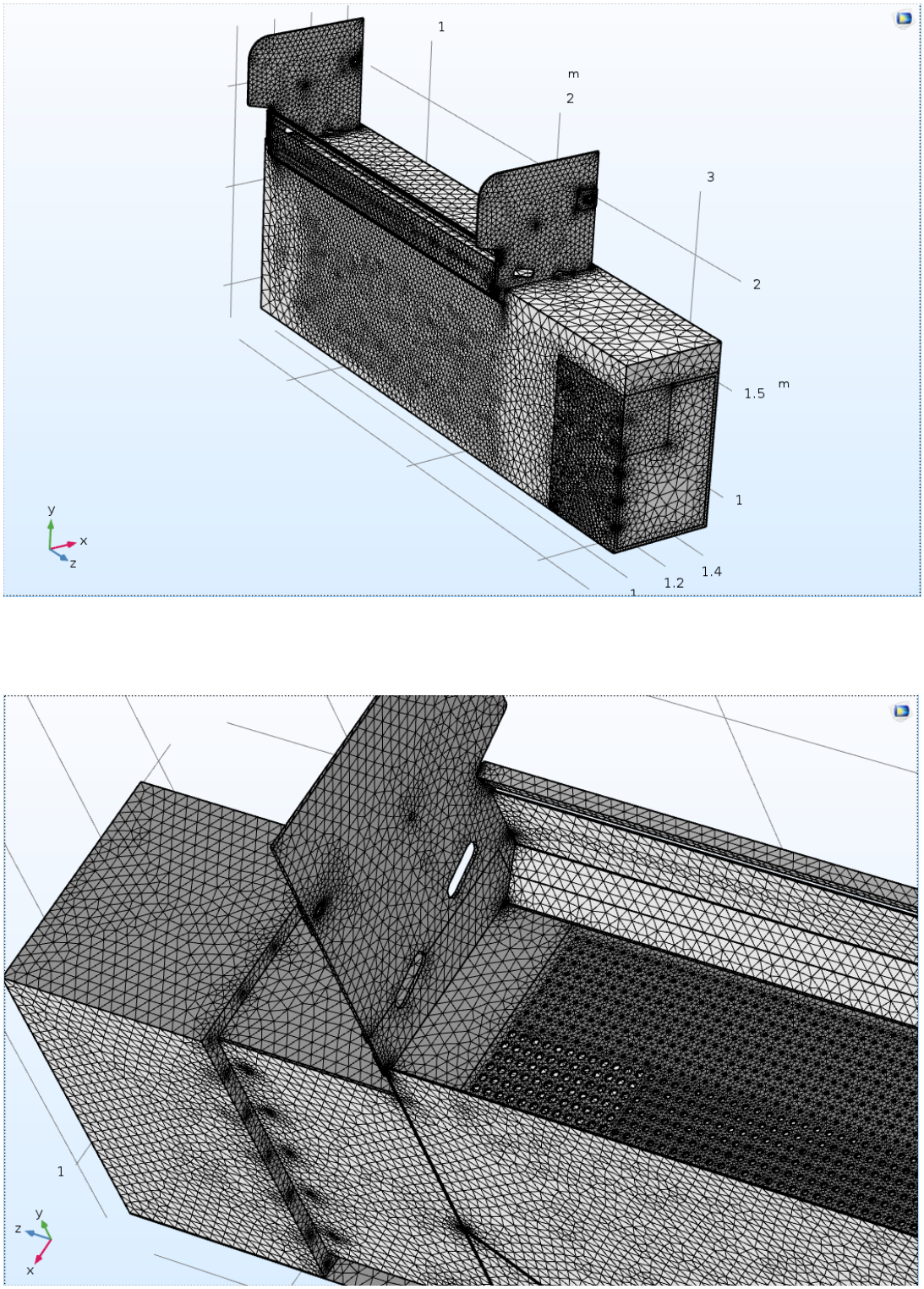

Figure 9. Three dimensional view of the air plenum with mesh generated by COMSOL physics controlled meshing, with a fine mesh size.

When a geometry is meshed, it is split into finite elements or control volumes, which are each solved for the conditions of flow at the center of each control volume. The commonly used volume meshes are the polyhedral and tetrahedral meshes. In addition to these meshes, there are prism, triangular and quad meshes. The tetrahedral mesh generates fewer volumes as opposed to a polyhedral mesh providing the same level of accuracy. In ideal cases using a prism mesh at the fan inlet and the air duct outlet will increase the accuracy of the results obtained [16].

2.2.4.5 Post Processor Solver Settings

A stationary study is carried out on the model for specified configurations, with the stationary solver employing the algebraic multigrid solver employing a fully coupled solver. In a fully coupled solver, the information passes on from one physics to another and the material properties of one physics affect the next physics to which it is passed to. The default solver settings can be changed from MUMPS to PARDISO or SPOOLES, which are all effective and produce similar results but vary in terms of the amount of core memory that they use. MUMPS and PARDISO store the solution out of core, thereby making them faster. A time dependant study can be helpful in developing an animated vision of our result but requires a much higher hardware requirement. In this thesis we make use a stationary study employing MUMPS solver in the algebraic multigrid solver.

2.2.5 Experimental work

Experiments were conducted on the rock separator to understand the flow pattern of air within the duct and thereby the cause of inefficient separation of rocks from potatoes. The study helps us make relevant changes to the design based on our CFD simulations and experimental findings. Owing to the inaccessibility of the other regions, the measurements carried out on the rock-separator was limited to the region above the air plenum and wave bed.

2.2.5.1 Measurements above the wave bed

The testing was carried out above the air plenum after the fan was relocated from the top and placed right at the inlet with a small extension. This is to allow the air flow to be more developed and uniform. Eliminating the two 90° bends in the air socket duct, showed major changes in the flow pattern as well as increase in volume flowrate. Specific measurements to quantify distribution to understand the behaviour of air flow

above the wave bed was carried. It was also studied theoretically using CFD. Measurement of velocity and pressure above the wave bed was done with the help of a pitot tube (Figure 10). The pitot tube was connected to a digital manometer by means of a plastic tube. Measurements were carried out for every 150 mm space above the wave bed to ensure accuracy and repeatability adequate number of trials were conducted for each setup. A flow meter was attached to the inlet of the fan section to find the static pressure as well as the total volume flowrate at the inlet of the fan (Figure 10).

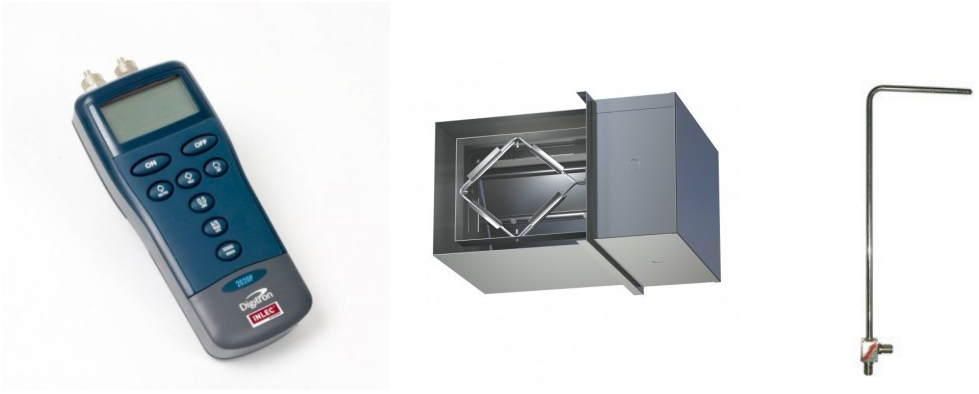

a) b) c)

Figure 10. a) Digital manometer, b) flow meter and c) pitot tube

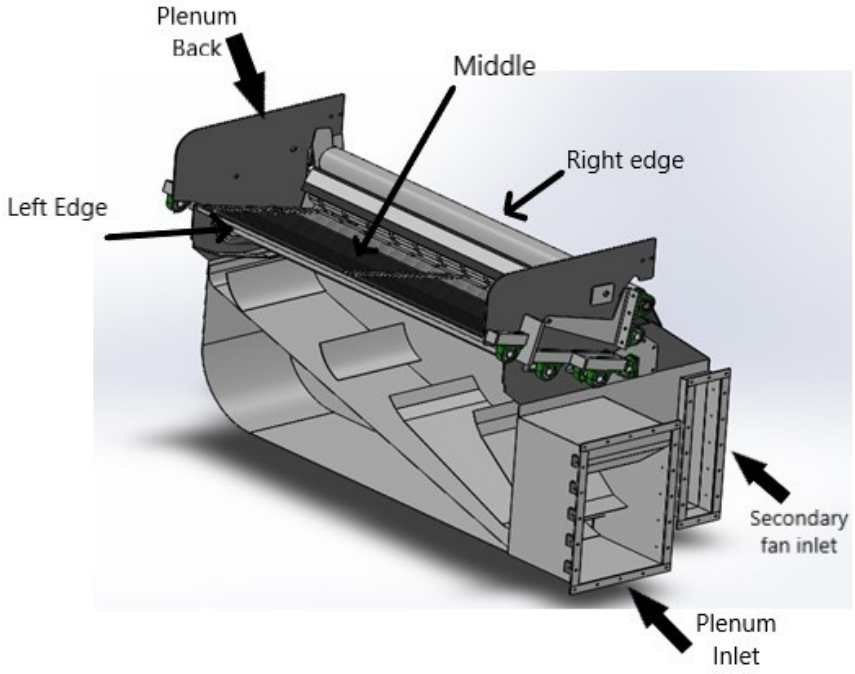

Figure 11. Three dimensional view of the Initial design of the separator with the wave bed and the baffles

2.2.5.2 Addition of perforated plate

Above measurements as well as the CFD analysis showed a large non uniformity of air flow above the wave bed even after the relocation of the fan. In an attempt to bring uniformity in levitation of potato above the wave bed, it was necessary to have air flow above the bed as uniform as possible. To achieve that, several tests were carried out by changing the air plenum design. This involved making changes to the baffle design, the extension and controlled blockage. None of the changes in the duct design achieved an adequately uniform air flow distribution above the wave bed. According to fluid dynamics principles flow uniformity is caused by varied fluid resistance across the duct cross section. An effective means of ensuring uniform flow among parallel fluid path is to put a new flow resistance significantly higher than the difference in resistance in the existing flow path. This practice is widely used in design of flow of water/steam in parallel tubes and grid design in fluidized beds. To apply this principle in duct, design a perforated plate was introduced between the air plenum exit and the wave bed, hoping to achieve flow uniformity. The perforated plate was made with 6.3 mm diameter holes equally spaced at 25.4 mm pitch on a thin plate covering the entire are of 1676 x 408 mm. It was uncertain what hole configuration will give best results, so for experimental purposes several plate configurations were tested. The initial layout is named Layout I. The measurements were carried out with the help of the pitot tube and manometer in three regions above the wave bed, named Left edge, middle and right edge (Figure 10).

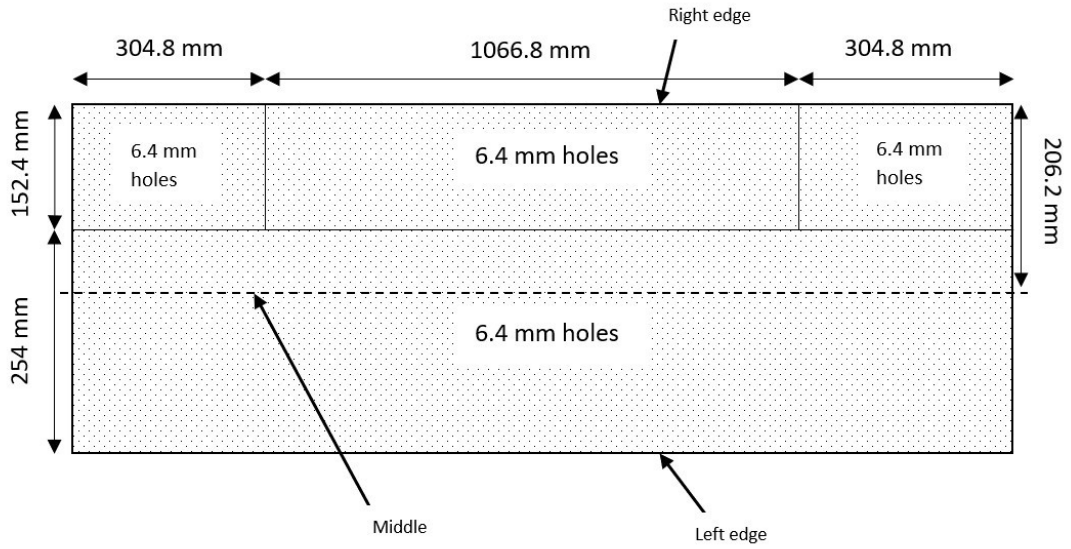

Figure 12. Plan view of Layout I version of the perforated plate

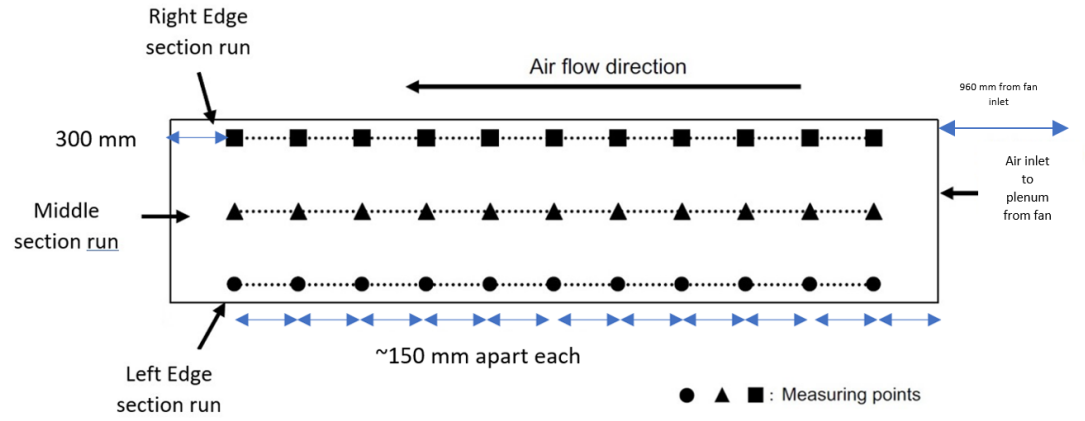

Figure 13. Measurement points for local velocity shown on the plan view of the perforated plate

2.2.5.3 Hole size adjustments in the perforated plate

The introduction of the perforated plate improved the uniformity of the air distribution, but few regions showed non-uniformity, so it required alteration in hole size in those specific regions of the perforated plate. The perforated plate in the right edge was divided into three regions, as shown in Figure 14, and in total there were four divided regions in the perforated plate. The holes for the regions which showed lower velocity was increased.

With the desired uniformity required, perforations were made on the plate to achieve our needs. The section 1 of the plate had holes in the size diameter of 9.5 mm and the section 2 had a mix of 9.5 mm and 6.4 mm. The section 3 which required the most air supply had holes in the size of 12.7 mm. The section 4 did not have any changes made to hole size (Figure 14).

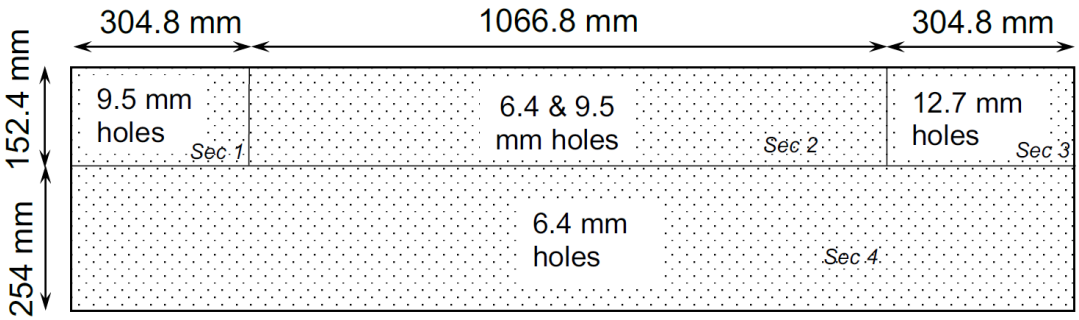

Figure 14. Plan view of Layout II of the perforated plate with varying hole size distribution

2.2.5.4 Removal of the Wave bed

The wave bed was removed from the air plenum to measure the velocity directly above the perforated plate (Figure 15). Removing the wave bed permits direct access to the plenum for measuring the pressure difference across the perforated plate. This improved the accuracy of assessing the velocity distribution for uniformity. The velocity pressure (m/s) was measured at a short distance right above the perforated plate and along its length. An increase in the velocity pressure was observed when the testing was done right above the perforated plate. The testing was done along the plate in the left edge, middle and right edge.

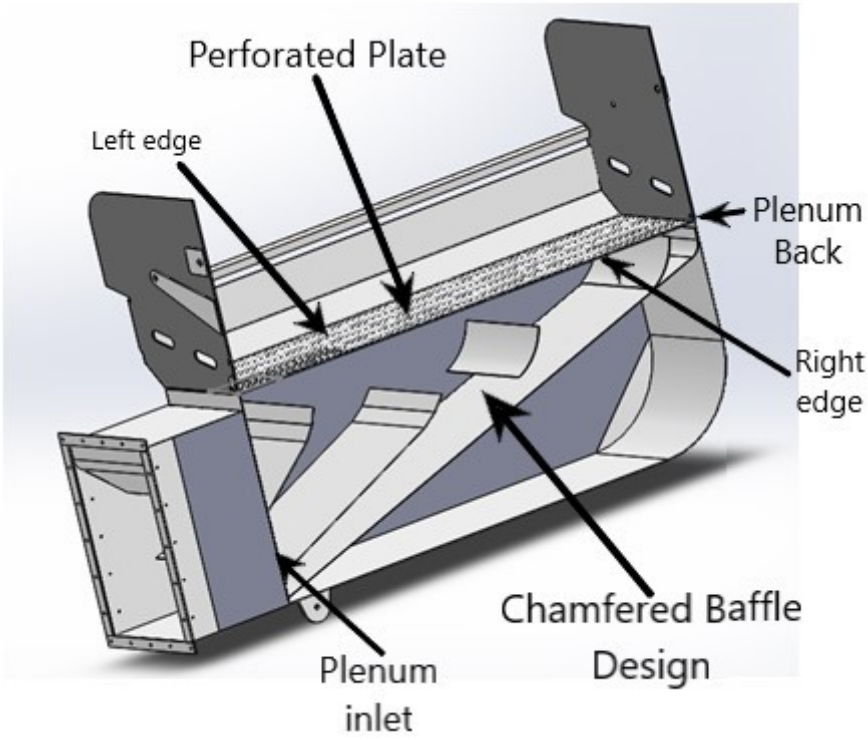

Figure 15. The air plenum with wave bed-with chamfered baffles-with perforated plate

2.2.5.5 Removal of the Baffles from the air plenum

The introduction of the perforated plate enhanced the flow uniformity, but it was uncertain whether this was the combined effect of baffle and perforated plate, so to understand the significance of the presence of baffles in the air plenum. They were removed and, with the perforated plate as shown in Figure 16, tests were carried out without the baffles in the three regions. The impact of removing the baffles was studied. The pitot tube was traversed across the perforated plate to measure the velocity pressure with the help of the digital manometer.

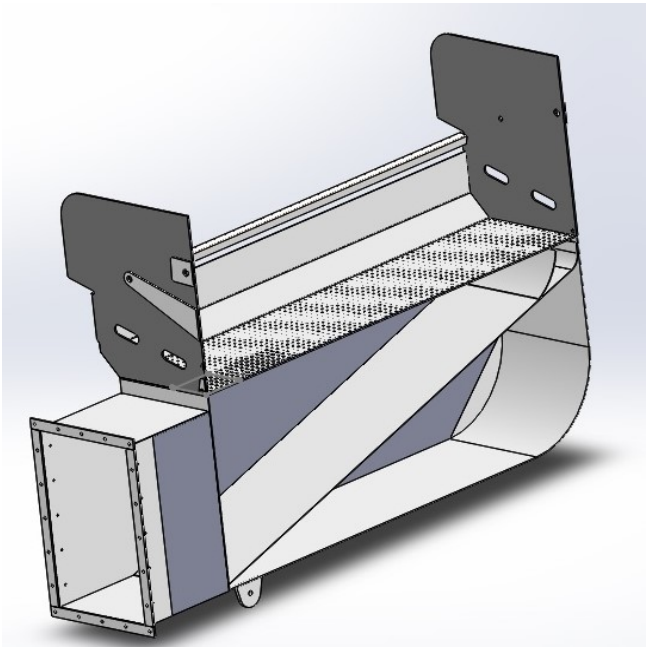

Figure 16. The air plenum without wave bed, without baffles but with perforated plate

2.2.5.6 Increase in the hole size of the perforated plate

Above measurements established that air flow uniformity of the system can be achieved with the help of the perforated plate, but the flow characteristics that is required to levitate the lower density particle, for the current design did not depend on a totally uniform velocity profile. It required higher velocity in certain regions (the right edge). Increasing the perforation size can help however achieving this criterion of selective flow uniformity. Increasing the hole size more than a permissible limit (above 20 %) however can affect the pressure drop and flow distribution across the bed and results in the loss of the required uniformity [18], [19]. Additionally, balance between increased flow rate and acceptable pressure drop (achieved by changing fractional opening) is one of the key factors that would help in improving the system's separation capability. Keeping the hole size, as shown in Layout II (Figure 14) has reduced the total flow rate because of the higher overall resistance on the centrifugal fan. The acceptable fractional opening percentage of the total area of the perforated plate was found to be in the range of 18-20 % [18].

Fractional opening of Layout II

To obtain the required air flow distribution size of holes and their numbers were changed in different locations. Table 1 shows the void area for each section; Table 2 shows the calculated percentage open area.

The measurement of velocities above the perforated plate was conducted in the absence of the wave bed and increased perforation (hole) size. To measure the total air flow rate, a diamond type duct-flow meter (Figure 10) was installed at the inlet of the suction section of the fan. The large resistance offered by the addition of the flow duct meter, however, greatly reduced the air flow rate from the centrifugal fan. The fractional opening size for Layout II was calculated to be 7 %. Such a low fractional opening meant that the holes can be increased further, thereby increasing the total flow rate as well. Hence the hole size was further increased in layout III (Figure 17).

Table 1. Layout II perforated plate hole size distribution

Section Ref: Figure 14	**No of holes**	**Hole diameter (mm)**	**Area (mm^2)**
1	72	9.5	5,101
2	252	7.9	12,346
3	72	12.7	9,116
4	680	6.4	21,864
Total open area in plate			**48,427 mm^2**

Table 2. Layout II fractional opening (Figure 14)

Plate length	1676	mm
Plate width	406	mm
Total area	681288	mm^2
Fractional Opening	**48427/681288 = 0.071**	

Fractional Opening for Layout III

The perforated plate's fractional opening was increased after running multiple CFD simulations and of its results. The opening was increased by 40 % of the existing hole size i.e. Layout II. The test was again carried out in the three regions along the perforated plate and considerable change was observed, in comparison with that of layout II. With the resistance reduced, the flow rate was increased. The sectional division of Layout III is shown in Figure 17.

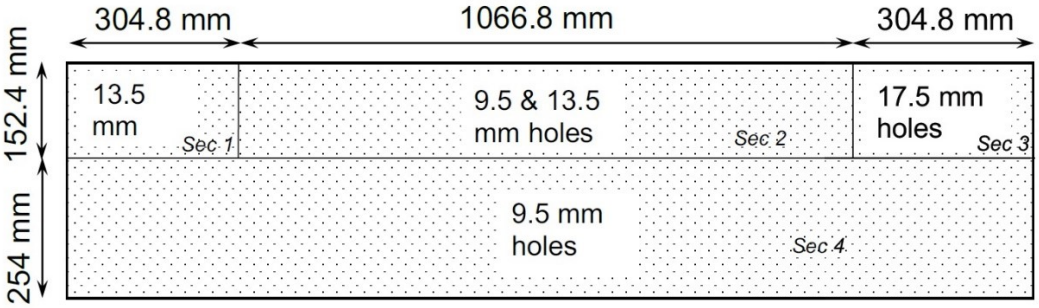

Figure 17. Layout III of the perforated plate

Table 3. Layout III perforated plate hole size distribution

Section Ref: Figure 17	No of holes	Hole size (mm)	Area (mm^2)
1	72	13.5	10295
2	252	11.5	26220
3	72	17.5	17250
4	680	9.5	48473
Total open area			**102,237 mm^2**

Table 4. Layout III (Figure 17) fractional opening

Plate length	1676	mm
Plate width	406	mm
Total area	681288	mm^2
Fractional Opening	**102237/681288 = 0.15**	

2.2.5.7 Re-attachment of the Wave bed

The wave bed is an integral part of the rock separation system as it assists in the separation process. In order to assess the system as a whole, the wave bed needed to be put back in place for taking the measurements from this point forward. The potatoes and rocks fall onto the wave bed which is placed just few millimeters above the perforated plate. The perforated plate is now made in such a way that more air is supplied to the right edge, where the rock separation mainly takes place. This is achieved by the use of the wave bed bars with rubber linings of different sizes (Figure 7). The rubber linings of different sizes vary the space between bars, through which air passes. The inclination of the wave bed towards the back ensures that the heavier rocks move towards the exit at the back. Higher air velocity at the back levitate potatoes there. In the inclined bed, more air flow at the back and the wave action of the wave bed are three key factors that aid in the separation process. In order to fully understand the effect of fractional openings on top of the wave bed, experiments were carried out at the top of it. As in previous tests, all the three regions were subjected to testing

2.2.5.8 Increase in perforation and changes is arrangement in sections

The region below the wave bed has obstructions in the form of cams and rods helping in the wave action of the wave bed, that prevent the air from escaping through few regions, causing non uniformity. The loss of uniformity after attaching the wave bed required additional changes in the layout pattern and hole sizes. The section 2 of the perforated plate was made to be the same pattern as section 1. The design philosophy of AE required right edge region to have more air compared to that in the middle and left edge. The configuration was made in such a way that the right edge had more air supply than the middle region, and the middle region had more air supply than the front region. This upgrade would prevent the clogging up of the potatoes.

The hole sizes, in select sections, were further increased by 20 % above that of the Layout III. The modified layout patter in shown in Figure 18. The calculations were done for the fractional openings and was found out to be at round 17 %, well below the appreciable 20 %. The calculated results are shown in Table 5 and 6.

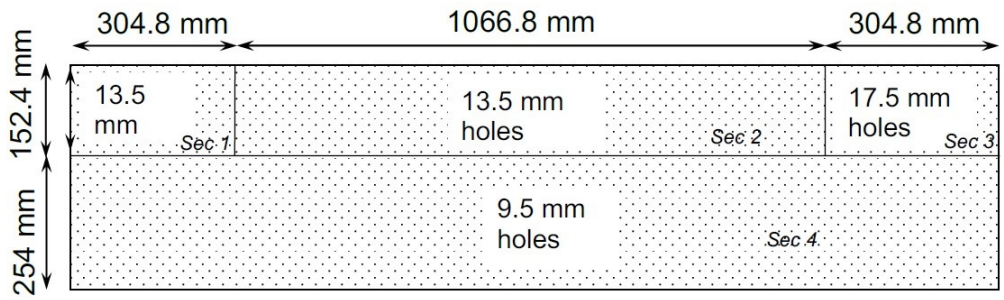

Figure 18. Layout IV of the perforated plate

Table 5. Layout IV perforated plate hole size distribution

Section Ref: Figure 18	**No of holes**	**Hole size (mm)**	**Area (mm^2)**
1	72	13.5	10,300
2	252	13.5	36,052
3	72	17.5	17,309
4	680	9.5	48,175
Total void area			**111,838**

Table 6. Layout IV fractional opening (Figure 18)

Plate length	1676	mm
Plate width	406	mm
Total area	681288	mm^2
Fractional Opening	**111838/681288 = 0.16**	

The fractional openings of the 4 layouts are listed in Table 7. The highest opening was fixed to be at 16 %

Table 7.The fractional opening percentage for each layout

Layout	Plan view	Fractional Opening Percentage (%)
I	Figure 12	4.92
II	Figure 14	7.11
III	Figure 17	15.00
IV	Figure 18	16.42

2.3 RESULTS AND DISCUSSION

This chapter discusses the results gathered through this research. The different experimental conditions, as discussed in chapter 2.2 were subjected to experimentation. The chapter covers the rock-potato separator part. In the section, we discuss the results of the air flow distribution above the wave bed and the various cases of study that were conducted to finally arrive at the conclusion. This final result is then compared with the CFD results, thereby establishing a relationship between the experimental and theoretical results. The velocity vs distance distribution is shown for different cases.

2.3.1 Case 1: Measurements above the wave bed – With Baffles – Without Perforated plate – Without Flowmeter

For the first case, the region above the wave bed was investigated. The purpose of this test was to understand the behavioural pattern of air flow above the wave bed region in the air bed. The test was done by placing a pitot tube, connected to a digital manometer, above the region and measuring the velocity pressure. The measurement was done by traversing the instrument along the entire length of the air plenum's exit above the wave bed and recording the readings every 150 mm. The right edge was measured for understanding the velocity discrepancies along the wave bed.

From the readings obtained it can be inferred that the air velocity above the wave bed was not uniform. The centre of the air duct appears to have a significantly low local velocity, although the plenum inlet and plenum back sections did show a much higher local velocity. This case is shown in Figure 19.

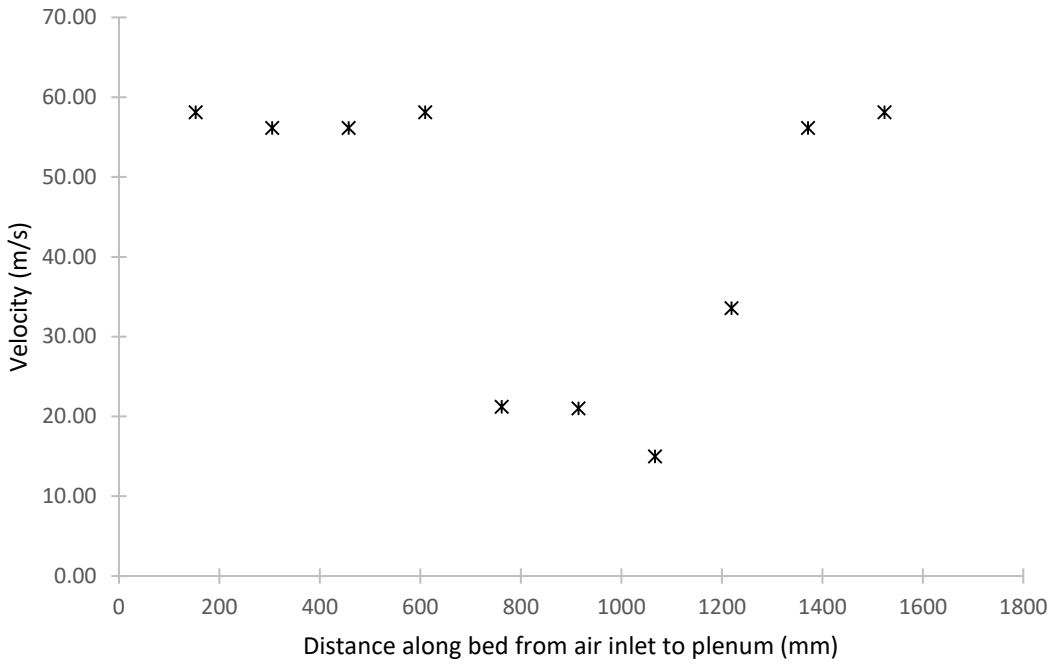

Figure 19. Experimental values of velocities measured along the length of the right side of the top of the wave bed (Figure 13b) in absence of perforated plate but with baffles in the plenum.

Table 8. Velocity measurements in the region above the wave bed

Distance along bed measured from plenum inlet (mm)	**Measured static pressure difference in pitot tube (Pa)**	**Calculated velocity (m/s)**
152	2068	58.11
305	1931	56.14
457	1931	56.14
610	2068	58.11
762	276	21.22
914	276	21.00
1067	138	15.00
1219	689	33.55
1372	1931	56.14
1524	2068	58.11

2.3.2 Case 2: Measurements Above Wave Bed - With Baffles - With Perforated Plate (Layout I) - Without Flowmeter

A perforated plate was introduced between the wave bed and the above the plenum. To achieve uniform air flow at the top of the air duct, this perforated plate was introduced between the wave bed and the baffle exit. The velocity at the exit, above the wave bed was tested using a pitot tube and a manometer. The perforated plate was made up of holes as shown in Layout I (Figure 12). The local velocity obtained from this test showed that, compared to what it was before (Fig 19) the velocity distribution above the wave bed is much more uniform. Even though there is some non-uniformity (Fig. 20) it is not as wide as before the perforated plate was introduced. The velocity was highest at the centre (Figure 20), which was lowest in the case 1 test (Figure 19).

One noticeable effect of introduction of the perforated plate was very large reduction in the average and peak velocity above the wave bed. The distribution of air at certain regions above the wave bed were not uniform and the velocity had drastically reduced. It is a direct result of high additional flow resistance offered by the perforated plate on the centrifugal fan,

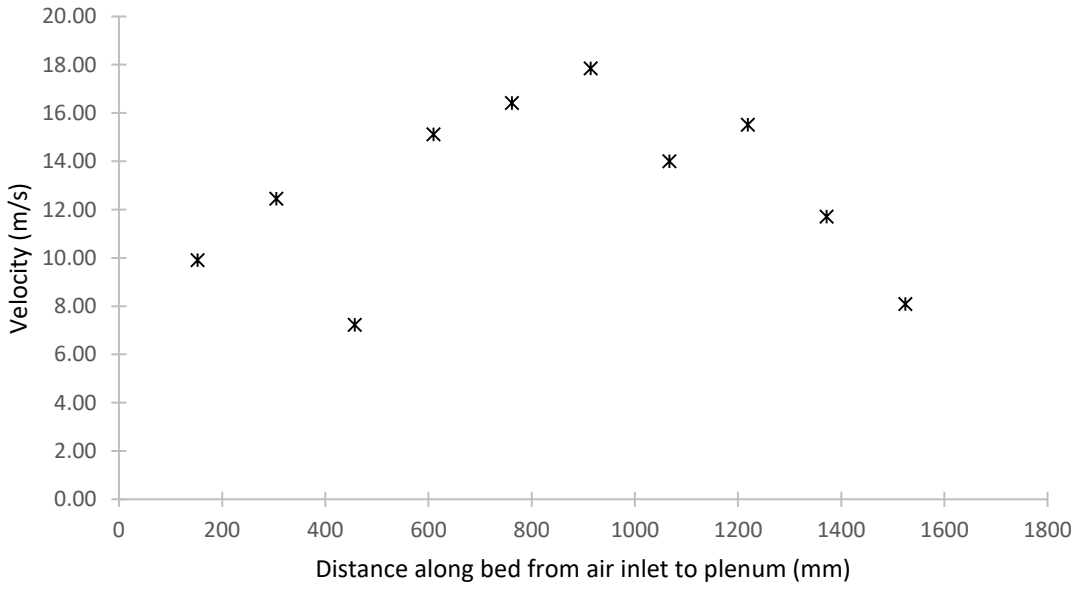

Figure 20. Velocities measured along the right edge of the wave bed with perforated plate in (Layout I) and with baffles.

Table 9. Velocity at the region above the wave bed with perforated plate (layout I) and chamfered baffles present (Fig 14)

Distance along the bed from plenum inlet	**Velocity pressure reading of pitot tube**		**Average velocity Pressure**	**Calculated Velocity**
	Trial #1	**Trial #2**	**Average**	
(mm)	(Pa)	(Pa)	(Pa)	(m/s)
152	60	60	60	9.90
305	50	140	95	12.45
457	44	20	32	7.23
610	150	130	140	15.12
762	160	170	165	16.41
914	110	280	195	17.84
1067	100	140	120	14.00
1219	125	170	147.5	15.52
1372	78	90	84	11.71
1524	40	40	40	8.08

2.3.3 Case 3: Measurements Above Wave Bed - With Baffles - With Perforated Plate (Layout II) - Without Flowmeter

Since the velocity of the air exiting through the plenum appeared to be non-uniform even after the introduction of the perforated plate, an increase in the hole size in specific sections was required. The perforated plate was subdivided into 4 sections. These 4 sections were made into perforations of different sizes, Layout II (Figure 14).

After the changes in hole size, the region above the wave bed was tested to find out the velocity pressure using a pitot tube. The pitot tube was traversed along the wave bed and the velocity pressure was measured. The local velocity obtained after the initial tests showed that the uniformity of the velocity had substantially increased (Figure 21) as compared to the previous case 2 (Figure 20).

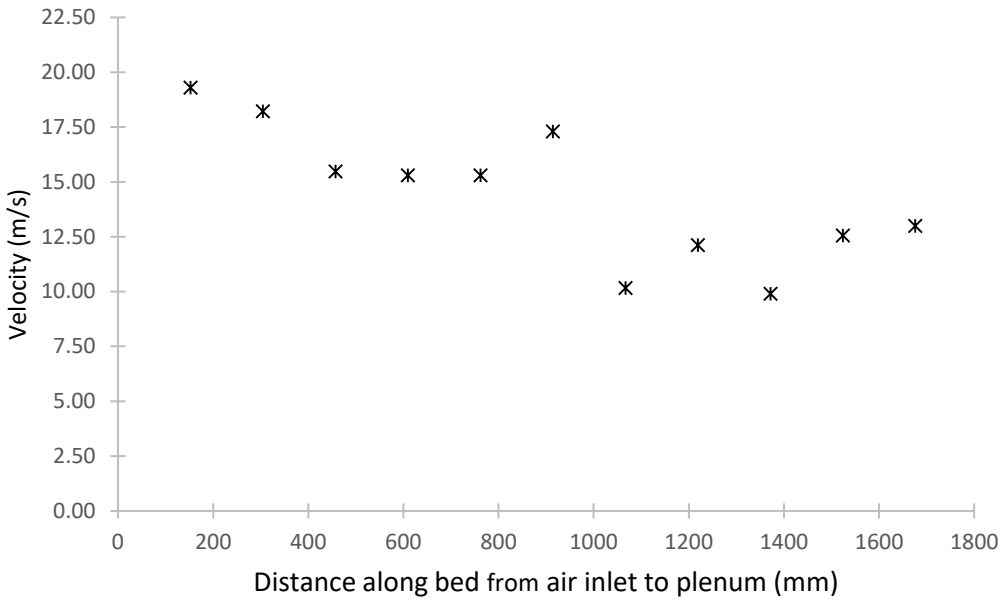

Figure 21. Velocities measured along the right edge of the wave bed with perforated plate (Layout II) and the baffles in plenum.

Table 10. Velocity at the region above the wave bed with perforated plate (layout II) and chamfered baffles present (Figure 14)

Distance along the bed from plenum inlet	**Pressure reading on pitot tube**			**Velocity Pressure**	**Velocity**
	Trial #1	**Trial #2**	**Trial #3**	**Average**	
(mm)	(Pa)	(Pa)	(Pa)	(Pa)	(m/s)
152	224	230	230	228	19.29
305	210	180	220	203.3	18.22
457	110	150	180	146.6	15.47
610	150	140	140	143.3	15.30
762	120	160	150	143.3	15.30
914	180	180	190	183.3	17.30
1067	60	50	80	63.3	10.17
1219	150	60	60	90	12.12
1372	80	50	50	60	9.90
1524	30	130	130	96.6	12.56
1676	80	100	130	103.3	12.99

2.3.4 Case 4: Measurements Above Perforated plate (Layout II) - With Baffles – Without Wave bed -With Flowmeter

The velocity pressure was measured at a distance right above the perforated plate and along it, in the right, middle and left sections. The perforated plate had the Layout II hole pattern (Figure 14). An increase in the velocity was observed when the test was done right above the perforated plate. The increase in the velocity, as expected was observed, since exit air velocity would increase with a reduction in the distance of testing, from the actual exit of air through the perforated plate. The velocity was more uniform above the perforated plate when compared with that measured above the wave bed. There were a few regions with non-uniformity which were observed (Figure 22).

To perform accurate CFD analysis the total volume flow rate is required, hence a flow meter was placed at the inlet of the centrifugal fan's suction section. The draft of the flow meter was of a radius of 12". The flow rate of air measured using a flow duct meter was 2.28 m^3/s. The pressure drop across the perforated plate was 1041 Pa.

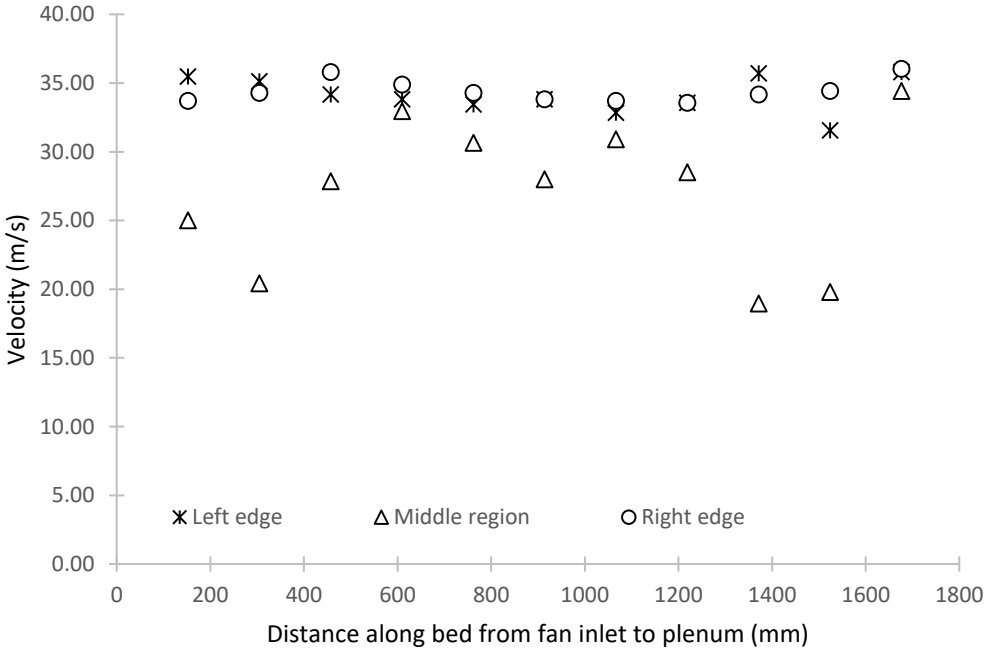

Figure 22. Measured velocities for different regions of the separator along the length of perforated plate. Layout II with the presence of baffles.

Table 11. Velocity at the Left edge, middle region and right edge above perforated plate w/ baffles

Distance along the bed from plenum inlet	**Left edge**				**Middle Region**			
	Pressure measured in pitot tube		Average Pressure	Velocity	Pressure measured in pitot tube		Average Pressure	Velocity
(mm)	Trial 1 (Pa)	Trial 2 (Pa)	(Pa)	m/s	Trial 1 (Pa)	Trial 2 (Pa)	(Pa)	m/s
152	780	760	770	**35.46**	380	386	383	**25.01**
305	730	780	755	**35.11**	260	250	255	**20.40**
457	700	730	715	**34.17**	450	500	475	**27.85**
610	700	700	700	**33.81**	600	730	665	**32.95**
762	680	690	685	**33.44**	550	600	575	**30.64**
914	700	700	700	**33.81**	500	460	480	**27.99**
1067	640	680	660	**32.83**	590	580	585	**30.90**
1219	690	690	690	**33.56**	500	495	497.5	**28.50**
1372	780	780	780	**35.69**	200	240	220	**18.95**
1524	600	620	610	**31.56**	200	280	240	**19.79**
1676	790	780	785	**35.80**	700	750	725	**34.40**

Distance along the bed from plenum inlet	**Right edge (Potato/rock entry side)**			
	Pressure measured in pitot tube		Average	Velocity
(mm)	Trial 1 (Pa)	Trial 2 (Pa)	(Pa)	m/s
152	690	700	695	**33.69**
305	720	720	720	**34.29**
457	780	790	785	**35.80**
610	740	750	745	**34.88**
762	720	720	720	**34.29**
914	700	700	700	**33.81**
1067	690	700	695	**33.69**
1219	690	690	690	**33.56**
1372	700	730	715	**34.17**
1524	740	710	725	**34.40**
1676	790	800	795	**36.03**

2.3.5 Case 5: Measurements Above Perforated plate (Layout II) – Without Baffles – Without Wave Bed - With Flowmeter

As observed in Section 2.3.4 case 4, the middle region of the perforated plate had a lower velocity when compared with the right and left edges. The test was carried out to examine the effect of baffles inside the air box. The layout of the perforation was the same as in Layout II. With the removal of the baffles inside, the test was carried out again. The test was carried out in three regions the Left edge, middle & right edge. The Pitot tube was traversed across the perforated plate and the velocity pressure was measured. The pressure difference across the perforated plate was also measured and found out to be 1040 Pa and the flow rate was found out to be 4834 CFM.

The uniformity of the air distribution had increased in all regions. The exit velocity from the plate was almost similar (Figure 23). With the removal of the wave bed it was found that the velocity was even more uniform.

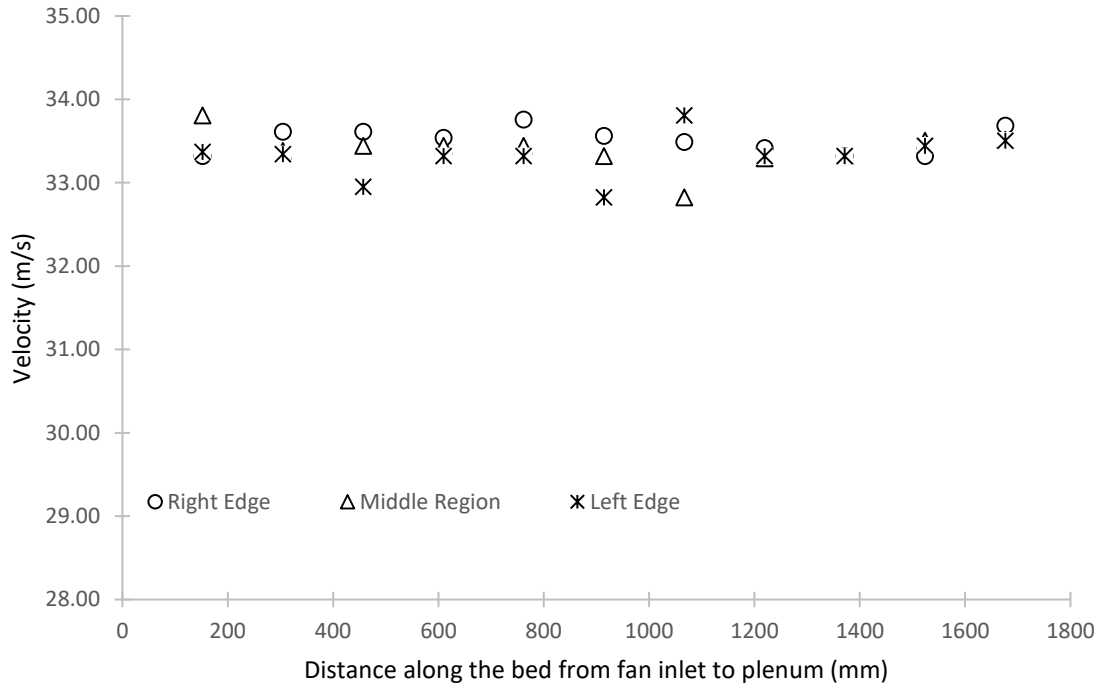

Figure 23. Measured velocities for different regions of the separator along the length of perforated plate. Layout II with flowmeter in the absence of baffles.

Table 12. Velocity at the Left edge, middle and right edge above perforated plate w/o baffles

Distance along the bed from plenum inlet	Left edge				Middle region			
	Pressure observed in the pitot tube		Average Pressure	Velocity	Pressure observed in the pitot tube		Average Pressure	Velocity
(mm)	Trial 1 (Pa)	Trial 2 (Pa)	(Pa)	m/s	Trial 1 (Pa)	Trial 2 (Pa)	(Pa)	m/s
152	680	684	682	**33.37**	700	700	700	**33.81**
305	680	682	681	**33.34**	680	685	682.5	**33.38**
457	660	670	665	**32.95**	690	680	685	**33.44**
610	680	680	680	**33.32**	680	690	685	**33.44**
762	680	680	680	**33.32**	690	680	685	**33.44**
914	640	680	660	**32.83**	690	670	680	**33.32**
1067	700	700	700	**33.81**	660	660	660	**32.83**
1219	680	680	680	**33.32**	680	678	679	**33.30**
1372	680	680	680	**33.32**	680	680	680	**33.32**
1524	690	680	685	**33.44**	685	690	687.5	**33.50**
1676	685	690	687.5	**33.50**	690	686	688	**33.52**

Distance along the bed from plenum inlet	Right Edge (Potato/rock entry side)			
	Pressure observed in the pitot tube		Average	Velocity
(mm)	Trial 1 (Pa)	Trial 2 (Pa)	(Pa)	m/s
152	680	680	680	**33.32**
305	694	690	692	**33.61**
457	690	694	692	**33.61**
610	690	688	689	**33.54**
762	700	696	698	**33.76**
914	680	700	690	**33.56**
1067	690	684	687	**33.49**
1219	680	688	684	**33.42**
1372	680	680	680	**33.32**
1524	680	680	680	**33.32**
1676	700	690	695	**33.69**

2.3.6 Case 6: Measurements Above Perforated plate (Layout III) – Without Baffles – Without Wave Bed - With Flowmeter

The analysis being focused on achieving the desired uniformity with a perforated plate, the required objective of uniformity was obtained. Although the flow of air through the exit of the plenum was uniform, the flow rate with which the air exited the perforated plate was not sufficient to lift the potatoes. Without adequate air flow at the exit, the desired separation of potato and rock would not be feasible. The size of the holes was further increased to study the effect of increasing the porosity of the plate.

The holes were increased in size by 20% and the setup was subjected to testing at the nominal fan setting i.e. 80 % load. The 20 % increase meant that the fractional opening of Layout I, increased from 7.11 % to 14.96 %. This hole pattern in Layout III (Figure 17). The flow rate was found out to be in the range of 4596 CFM and 6 in of water at the suction section. The increase in the holes size saw a drop in the velocity but produced an increase in the flow. This is because, an increase in the diameter of a hole outlet will increase flow and reduce the velocity. The changes in velocity can be observed in Figure 24.

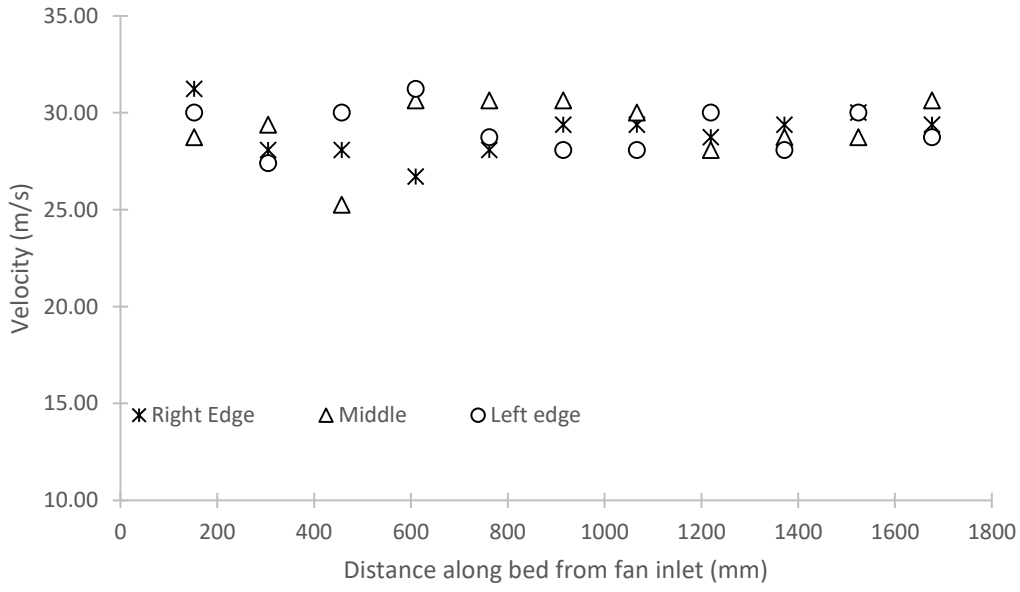

Figure 24. Measured velocities for different regions of the separator along the length of perforated plate. Layout III with flowmeter in the absence of baffles.

Table 13. Velocity at the Left edge, middle and right edge above perforated plate w/o baffles

Distance along the bed from plenum inlet	**Left Edge**					**Middle**				
	Pressure observed in the pitot tube			Average Pressure	Velocity	Pressure observed in the pitot tube			Average Pressure	Velocity
(mm)	Trial 1 (Pa)	Trial 2 (Pa)	Trial 3 (Pa)	(Pa)	m/s	Trial 1 (Pa)	Trial 2 (Pa)	Trial 3 (Pa)	(Pa)	m/s
152	552	552	552	552	**30.01**	483	621	414	506	**28.73**
305	414	552	414	460	**27.39**	552	552	483	529	**29.38**
457	414	621	621	552	**30.01**	414	345	414	391	**25.26**
610	552	621	621	598	**31.23**	621	552	552	575	**30.63**
762	552	414	552	506	**28.73**	621	552	552	575	**30.63**
914	483	483	483	483	**28.07**	552	621	552	575	**30.63**
1067	483	483	483	483	**28.07**	552	552	552	552	**30.01**
1219	552	552	552	552	**30.01**	483	483	483	483	**28.07**
1372	483	483	483	483	**28.07**	552	483	483	506	**28.73**
1524	552	552	552	552	**30.01**	483	552	483	506	**28.73**
1676	552	552	414	506	**28.73**	552	621	552	575	**30.63**

Distance along the bed from plenum inlet	**Right Edge (Potato/rock entry side)**				
	Pressure observed in the pitot tube			Average	Velocity
(mm)	Trial 1 (Pa)	Trial 2 (Pa)	Trial 3 (Pa)	(Pa)	m/s
152	552	621	621	598	**31.23**
305	483	552	414	483	**28.07**
457	552	414	483	483	**28.07**
610	414	345	552	437	**26.70**
762	483	483	483	483	**28.07**
914	414	621	552	529	**29.38**
1067	483	552	552	529	**29.38**
1219	414	552	552	506	**28.73**
1372	552	483	552	529	**29.38**
1524	483	621	552	552	**30.01**
1676	552	483	552	529	**29.38**

2.3.7 Case 7: Measurements Above Wave Bed (Layout III) – Without Baffles – With Perforated Plate - With Flowmeter

The uniformity of the system was achieved, and the wave bed was re-attached into the air plenum exit. The velocities were measured by traversing the pitot tube above the wave bed. The wave bed plays and integral part in the system and the reason for attaching the bed back to its default position and its significance was previously explained in Section 2.2.5.7.

The results obtained (Figure 25) after conducting the tests shows us that at some points along the bed there is slight discrepancies or loss of attained velocity. The probable reason for this occurrence could be due to the design or geometry of the wave bed, which could affect the air flow distribution above the wave bed. The various auxiliary fittings which house the wave bed in its position are assumed to cause this obstruction. The flow rate of the fan was found out to be 4596 CFM and the pressure drop was 600 Pa.

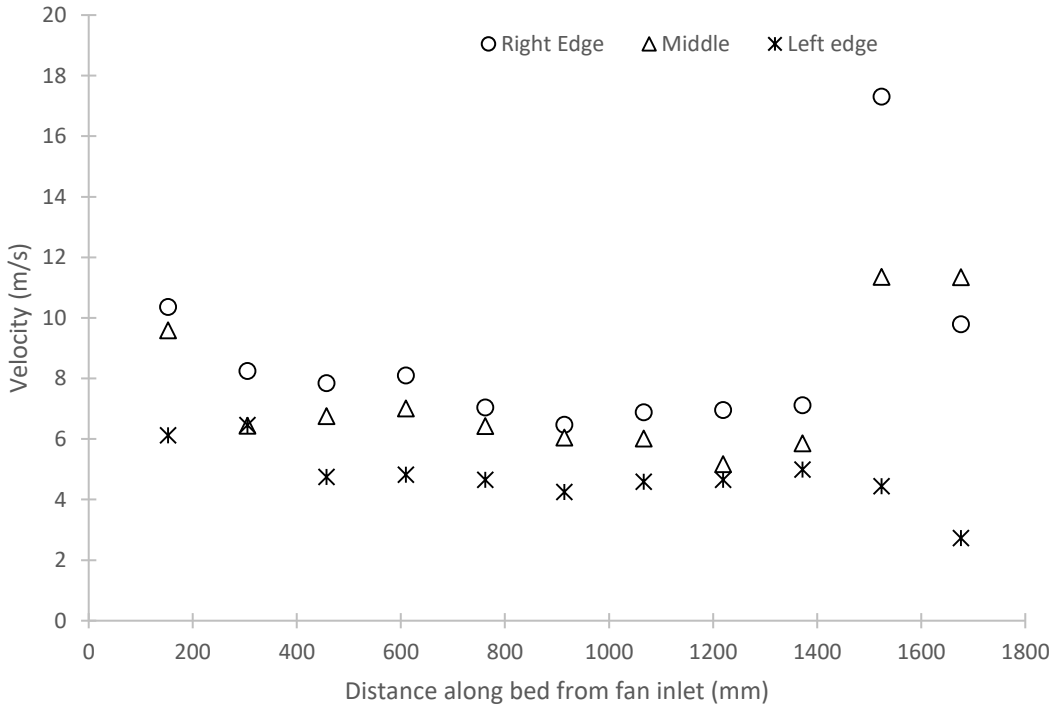

Figure 25. Measured velocities for different regions of the separator along the length of perforated plate. Layout III with flowmeter in the absence of baffles.

Table 14. Velocity at the Left edge, middle and right edge above wave bed w/o baffles

Distance along the bed from plenum inlet	Left Edge					Middle				
	Pressure observed in the pitot tube			Average Pressure	Velocity	Pressure observed in the pitot tube			Average Pressure	Velocity
(mm)	Trial 1 (Pa)	Trial 2 (Pa)	Trial 3 (Pa)	(Pa)	m/s	Trial 1 (Pa)	Trial 2 (Pa)	Trial 3 (Pa)	(Pa)	m/s
152	26	21	22	23	6.11	56	43	70	56	9.59
305	21	29	27	26	6.46	25	26	26	25	6.44
457	14	13	14	14	4.75	29	22	33	28	6.75
610	10	17	17	14	4.81	29	27	34	30	7.00
762	12	14	14	13	4.65	23	30	23	25	6.43
914	11	12	11	11	4.24	20	22	25	22	6.05
1067	9	14	15	13	4.58	23	24	20	22	6.02
1219	17	11	12	13	4.65	19	17	13	16	5.16
1372	16	15	15	15	4.99	19	27	17	21	5.86
1524	13	11	12	12	4.44	85	61	91	79	11.35
1676	4	4	6	5	2.73	75	57	104	79	11.34

Distance along the bed from plenum inlet	Right Edge (Potato/rock entry side)				
	Pressure observed in the pitot tube			Average	Velocity
(mm)	Trial 1 (Pa)	Trial 2 (Pa)	Trial 3 (Pa)	(Pa)	m/s
152	44	53	100	66	10.35
305	44	38	43	42	8.25
457	35	38	40	38	7.84
610	35	39	46	40	8.09
762	25	37	29	30	7.04
914	23	32	22	26	6.46
1067	29	30	28	29	6.88
1219	30	31	28	30	6.96
1372	25	38	30	31	7.11
1524	190	180	180	183	17.30
1676	50	70	56	59	9.79

2.3.8 Case 8: Measurements Above Wave Bed (Layout IV) – Without Baffles – With Perforated Plate - With Flowmeter

As per the client demands, the right edge of the wave bed, which is inclined downward required more air flow, followed by the middle and left edges. This is done in order to achieve efficient separation of the potatoes and rocks.

To account for the variation in velocity caused due to the re-fitting of the wave bed and to allow more air flow though the right edge, an analysis of the design/layout of the perforated plate was required. The hole size and pattern were changed from the previous layout III, and a new layout IV (Figure 17) was introduced to achieve uniform flow distribution in the said areas lacking air flow thereof. The flow meter, still in position was used to find out the flow rate (4834 CFM). The pressure-drop also reduced to 520 Pa.

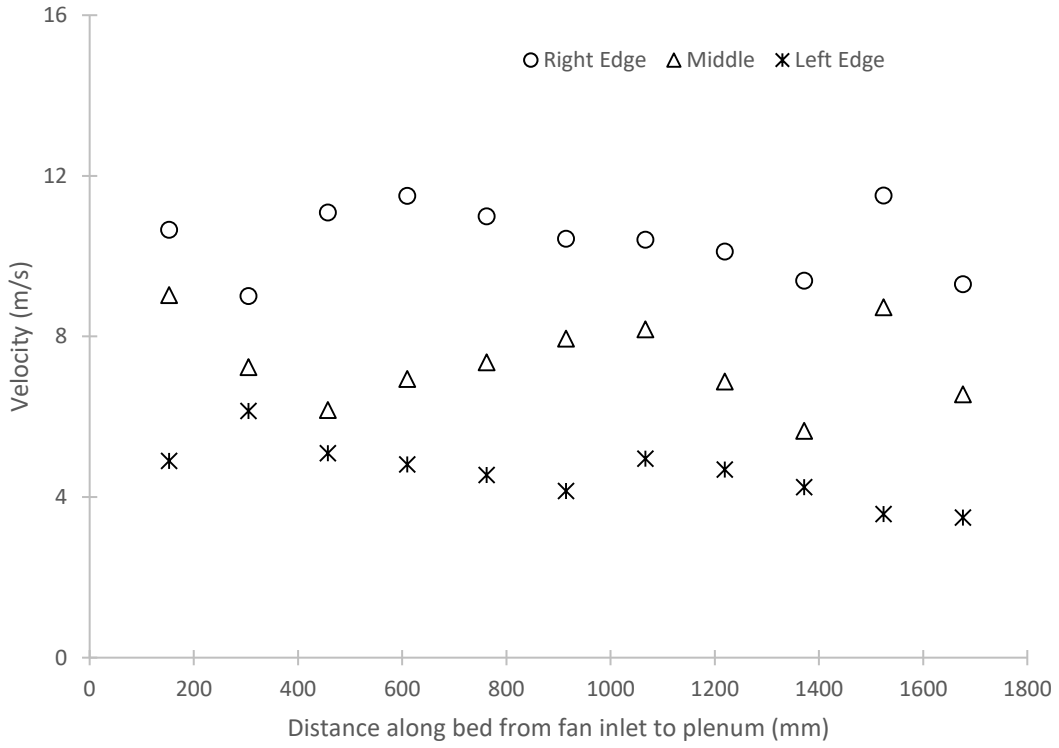

Figure 26. Measured velocities for different regions of the separator along the length of perforated plate. Layout IV with flowmeter in the absence of baffles.

Table 15. Velocity at the Left edge, Middle and Right edge above wave bed w/o baffles

Distance along the bed from plenum inlet	**Left edge**					**Middle**				
	Pressure observed in the pitot tube			Average Pressure	Velocity	Pressure observed in the pitot tube			Average Pressure	Velocity
(mm)	Trial 1 (Pa)	Trial 2 (Pa)	Trial 3 (Pa)	(Pa)	m/s	Trial 1 (Pa)	Trial 2 (Pa)	Trial 3 (Pa)	(Pa)	m/s
152	18	13	13	15	4.90	42	58	50	50	**9.03**
305	26	25	18	23	6.14	33	33	30	32	**7.24**
457	16	16	16	16	5.10	23	23	24	23	**6.17**
610	15	14	14	14	4.81	42	23	24	30	**6.94**
762	12	13	13	13	4.55	38	34	27	33	**7.35**
914	11	11	11	11	4.15	35	34	47	39	**7.95**
1067	16	13	16	15	4.95	56	57	10	41	**8.18**
1219	12	14	14	13	4.69	33	29	25	29	**6.88**
1372	10	12	12	11	4.25	32	11	15	20	**5.65**
1524	9	9	6	8	3.58	38	41	61	47	**8.73**
1676	8	7	7	7	3.49	19	16	44	26	**6.56**

Distance along the bed from plenum inlet	**Right edge (Potato/rock entry side)**				
	Pressure observed in the pitot tube			Average	Velocity
(mm)	Trial 1 (Pa)	Trial 2 (Pa)	Trial 3 (Pa)	(Pa)	m/s
152	70	60	79	70	10.65
305	40	53	56	50	9.00
457	78	78	70	75	11.09
610	77	83	83	81	11.50
762	84	62	76	74	10.99
914	58	78	64	67	10.43
1067	71	62	66	66	10.41
1219	64	56	68	63	10.11
1372	54	54	54	54	9.39
1524	70	86	87	81	11.51
1676	55	54	50	53	9.30

2.3.9 Case 9: Measurements Above Wave Bed (Layout IV) – Without Baffles – With Perforated Plate - Without Flowmeter

The flow resistance was reduced by removing the flow duct meter placed at the centrifugal fan inlet and thereby increasing the flow rate of air. The isolation of the flow meter from the suction section of the fan is to record the velocity at which the harvester will function under ideal load conditions in the field. The velocity measurements were conducted above the wave bed with the perforated plate of Layout IV (Figure 17). The velocity distribution pattern showed little to no change, while the magnitude of the velocity had slightly increased from the previous case.

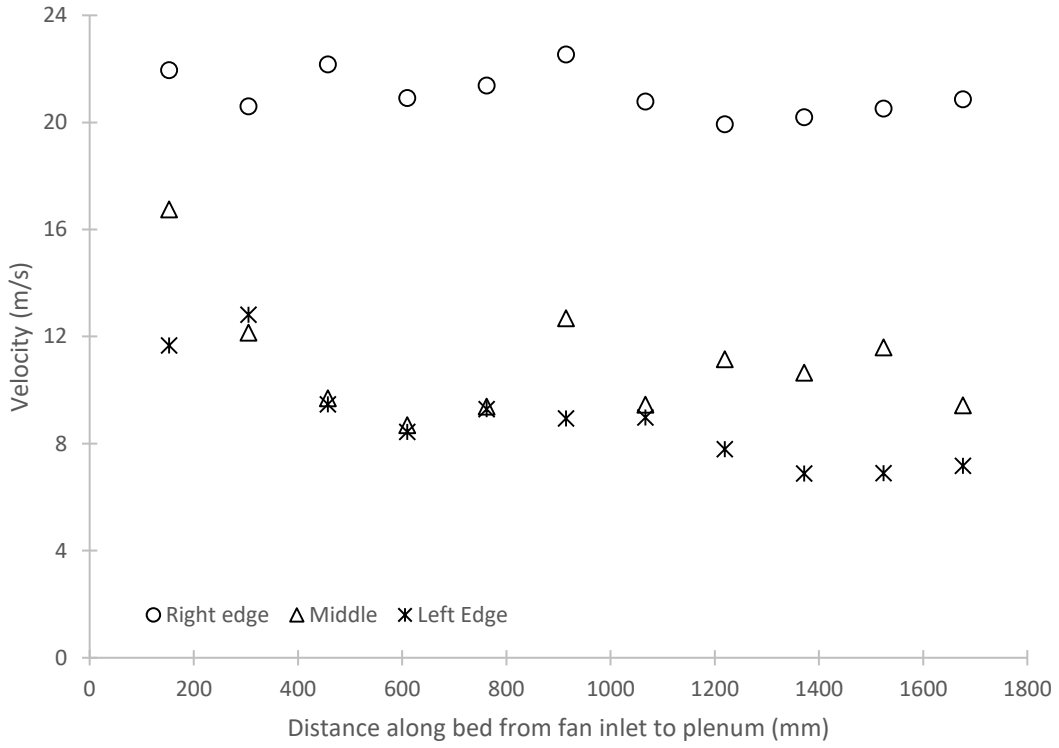

Figure 27. Measured velocities for different regions of the separator along the length of perforated plate. Layout IV without flowmeter in the absence of baffles.

Table 16. Velocity at the Left edge, middle and right edge above wave bed w/o flowmeter

Distance along bed (X)	**Left Edge**					**Middle**				
	Pressure observed in the pitot tube			Average Pressure	Velocity	Pressure observed in the pitot tube			Average Pressure	Velocity
(mm)	Trial 1 (Pa)	Trial 2 (Pa)	Trial 3 (Pa)	(Pa)	m/s	Trial 1 (Pa)	Trial 2 (Pa)	Trial 3 (Pa)	(Pa)	m/s
152	92	68	90	83	11.67	150	186	180	172	16.75
305	100	102	100	101	12.82	96	84	91	90	12.15
457	56	53	56	55	9.48	52	59	62	58	9.70
610	49	37	45	44	8.44	41	56	42	46	8.69
762	54	52	53	53	9.29	50	62	50	54	9.39
914	51	45	51	49	8.95	106	100	90	99	12.69
1067	53	42	53	49	8.97	60	57	48	55	9.46
1219	38	36	38	37	7.80	90	85	54	76	11.16
1372	27	30	30	29	6.89	55	93	61	70	10.66
1524	28	30	30	29	6.90	67	100	80	82	11.59
1676	30	33	32	32	7.17	50	63	50	54	9.43

Distance Along bed (X)	**Right Edge (Potato/rock entry side)**				
	Pressure observed in the pitot tube			Average	Velocity
(mm)	Trial 1 (Pa)	Trial 2 (Pa)	Trial 3 (Pa)	(Pa)	m/s
152	286	300	300	295	**21.96**
305	260	280	240	260	**20.60**
457	323	290	290	301	**22.17**
610	258	273	273	268	**20.92**
762	240	300	300	280	**21.38**
914	318	308	308	311	**22.55**
1067	264	265	265	265	**20.79**
1219	240	260	230	243	**19.93**
1372	250	260	240	250	**20.20**
1524	250	262	262	258	**20.52**
1676	240	290	270	267	**20.87**

2.3.10 Comparison of experimental with simulation results

The Computational fluid dynamic software, COMSOL was used to find the best possible design simulation. These boundary conditions for the simulation were obtained by keeping the fan setting at initial load conditions and measuring the value of velocity with which air exits through the centrifugal fan. The simulations were also used to find out the best possible design configuration by using appropriate boundary condition. These boundary conditions were obtained by keeping the fan setting at initial load conditions and measuring the value of velocity with air exits from the centrifugal fan. Thus, the need for hardware changes in the rock separator was avoided, thereby saving usage of raw materials and manpower.

In the initial condition wherein, the fan was located above the harvester, requiring the air flow to take two 90 degree bends, a rough simulation with the fan outlet velocity was conducted and the streamlined velocity pattern was obtained. As seen from Figure 28, we can see that the region right at the inlet section of the duct/the first and second baffles received less to no air. The fan was moved to the inlet section to negate the two 90 degree bends, shown in Figure 29.

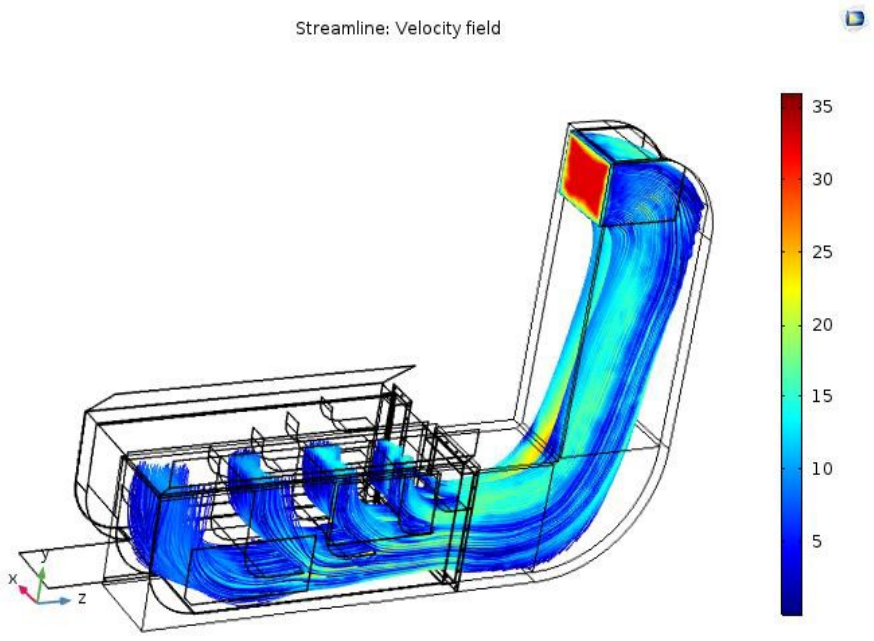

Figure 28. The initial streamlined velocity prediction for the harvester's air duct

Figure 29. The fan moved from the top of the harvester and mounted at the inlet of the plenum

Figure 30 shows the region above the bed when the baffles, the wave bed and the perforated plate are not present. This condition shows that without any resistance and the fan attached at the inlet, the velocity with which air exits the bed is concentrated at the back and substantially lesser at the fan inlet side. This design shows non-uniform air flow and hence leading to inefficient separation. This simulation was run at a lower velocity of 33 m/s as opposed to the nominal velocity (43 m/s) with which the fan operates.

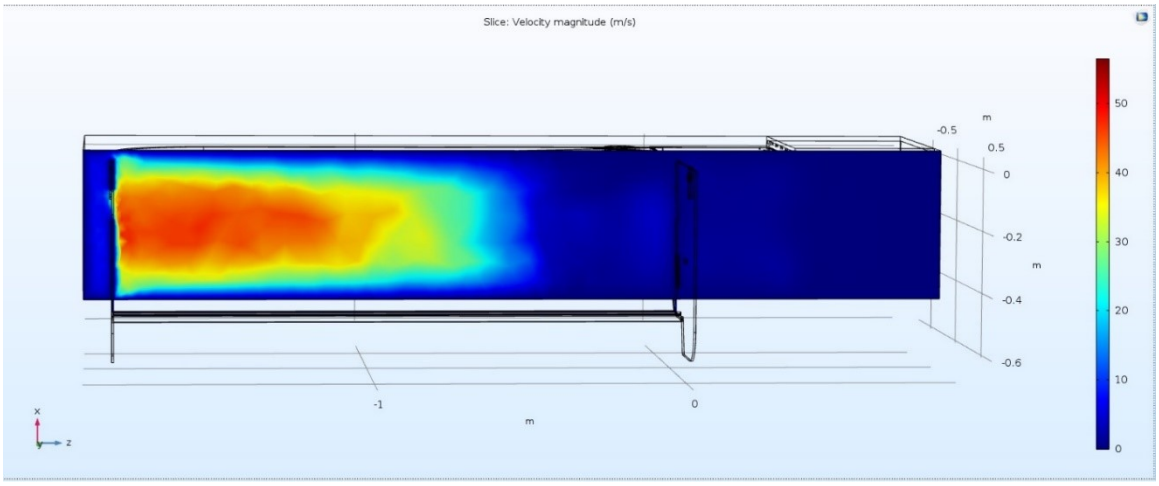

Figure 30. Simulated velocity distribution above the air chamber with no perforated plate & baffles

The velocities at region above the wave bed was computed using the commercial CFD code of COMSOL whose results are shown in Figure 31. These results were compared with those measured on the full scale unit. Figure 32 shows a reasonably good correlation between the flow predicted by CFD simulation and that measured. This verified validity of the present simulation.

For simulation, the initial boundary conditions and the turbulence condition have ben specified for the k-ε model. Parameters such as the turbulent intensity and turbulent length scale can be determined with the help of the turbulent kinetic energy. The modelling method employed was the RANS turbulence flow model. The parameters were chosen based on previous studies, showing the difference in computational cost when switching between different models for CFD analysis. The figures shown here are for a few conditions in which the simulations results matched the physically conducted experiments.

Figure 31 shows the region above the bed when the baffles, the wave bed and the perforated plate are not present. In This condition there is less resistance and the fan mounted at the inlet. The far side region leading away from the fan is subjected to more flow and the center. This design shows non-uniform air flow and hence resulting in the inefficient separation of potato and rocks, similar to the previous test condition shown in Figure 30.

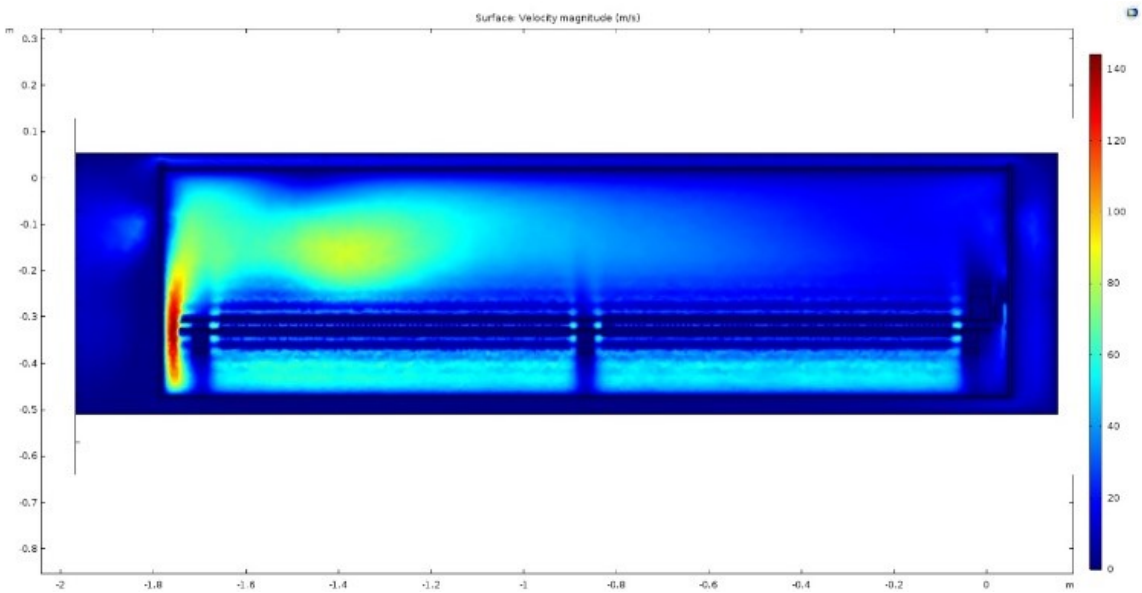

Figure 31. Simulated velocity distribution above the air chamber with no perforated plate & baffles

The simulation was carried out with both baffles and the wave bed but without the perforated plate. A comparison between experimental and COMSOL values for this condition is shown in Figure 22. Based on the fan setting at 80%, the velocity of air coming through the inlet was kept at 43 m/s. Since there is no perforated plate, the velocity is high as indicated in the velocity scale. This comparison shows that the CFD simulation accurately predicts the pattern of a dip in velocity in the centre portion of the right end.

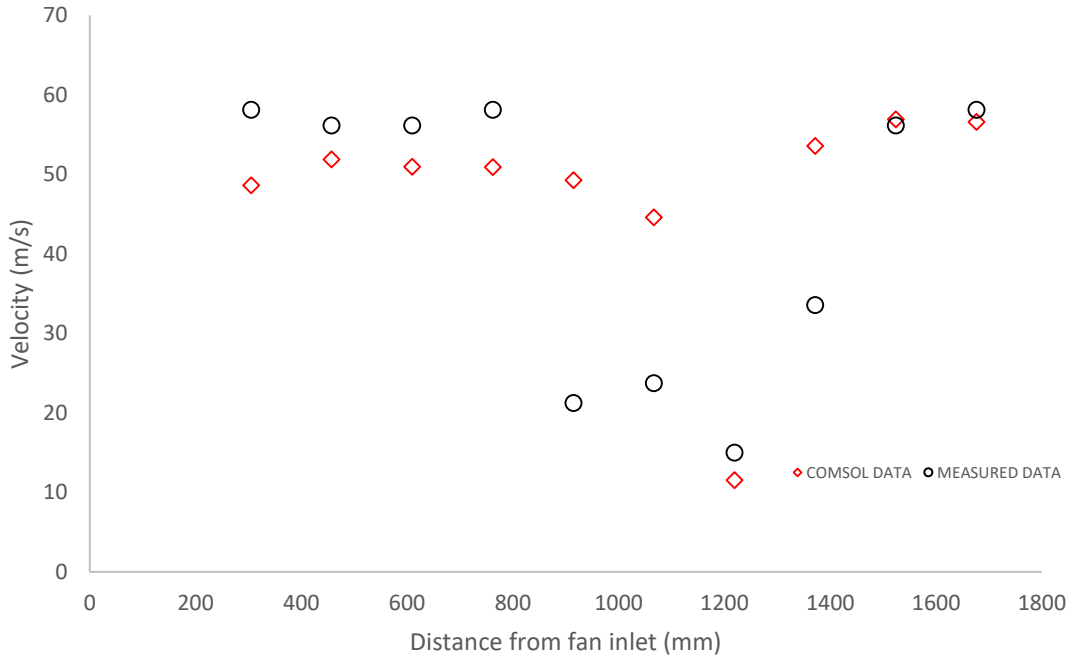

Figure 32. Comparison of Simulated and experimental values of velocity above the wave bed with baffles and without the plate.

A simulation was run for the layout III and this is compared with the experimental results in Figure 34, which shows that the CFD result closely resembles and matches with the measured values at the right edge. The velocity pattern is shown in Figure 33. The analysis was carried out in the region above the perforated plate and hence the simulation's velocity profile is obtained at the region right above the perforated plate.

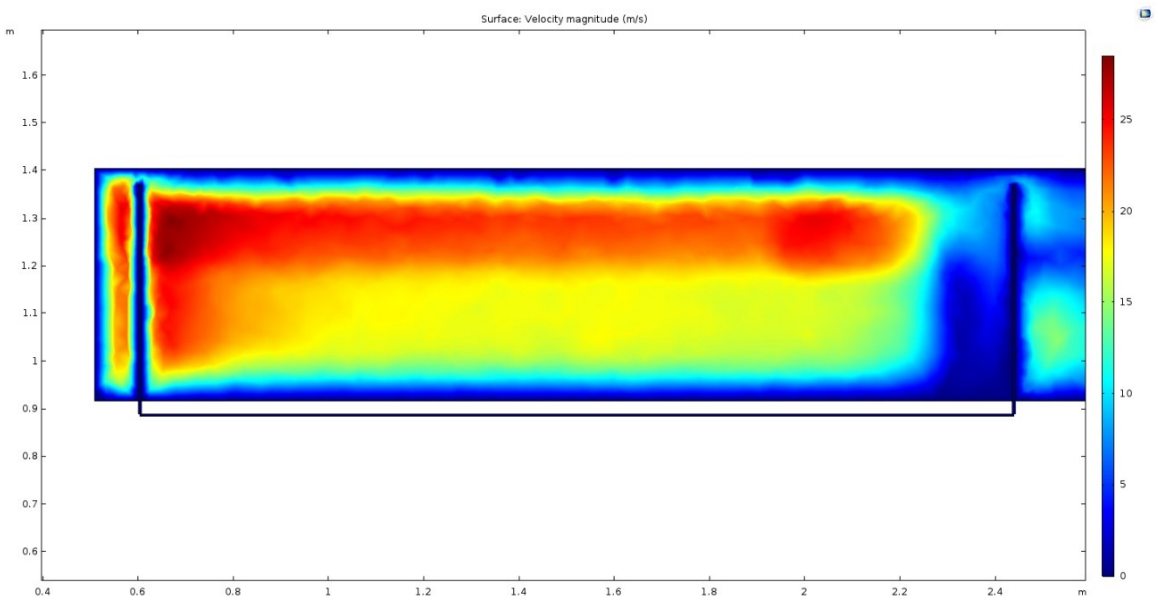

Figure 33. Simulated velocity distribution above the air chamber with the perforated plate and no baffles

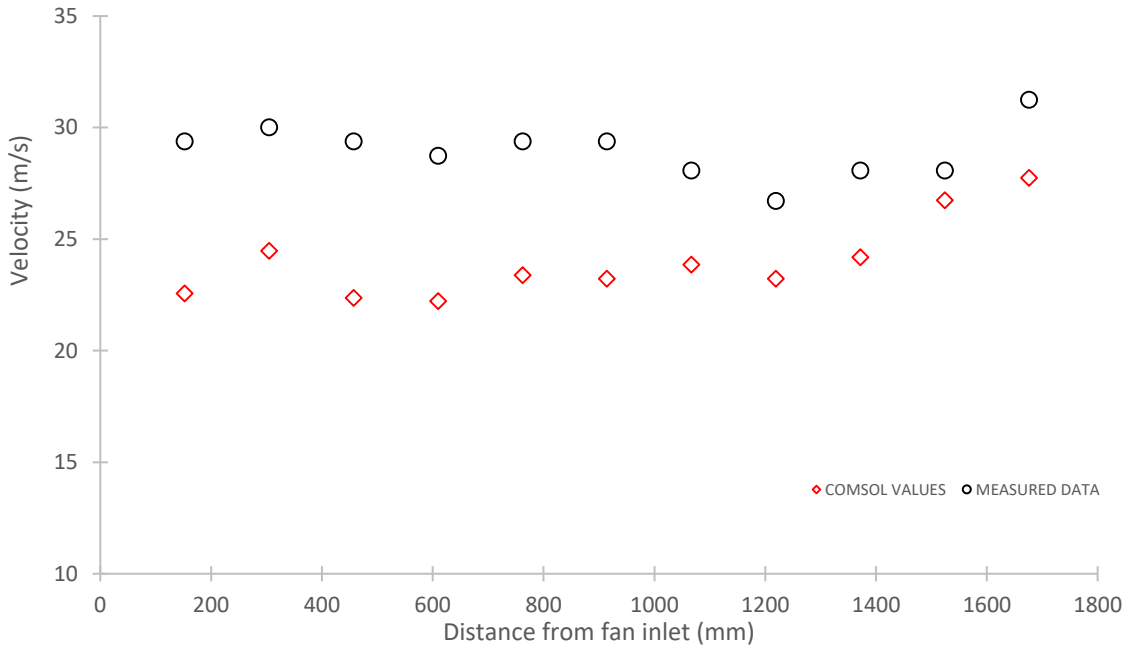

Figure 34 Comparison of predicted and experimental values of velocity above the perforated plate without the baffles

2.4 SUBCONCLUSIONS

1. This work was aimed at helping the Allan Equipment (AE) of PEI improve their existing design of the potato-rock separator, and this objective was achieved by providing the desired air velocity distribution above the air plenum.
2. CFD simulation of velocity distribution was validated against experimental results obtained at Alan Equipment factory in their full scale model
3. CFD simulation suggested two modifications a) relocation of the fan and b) addition of a perforated plate on the air plenum
4. Design changes made, improved the velocity distribution as predicted by CFD.
5. AE wanted further improvement of more air flow on one side than other.
6. Series of trials were made by changing the sizes of perforation hole and their distribution on the plate. Experimental measurements on each of these plates found that the design Layout IV gave the best results conforming to AE's need.

Chapter 3: DEVELOPMENT OF NEW DESIGN

3.1 DEVELOPMENT STRATEGY

Improved design of the airbox could take AE's design of the separator only to a certain level. For more advanced separation more advanced and novel means of separation needs to be developed. We considered using a gas-solid fluidization technique as an appropriate means for development because of its unique advantages as listed by Basu [20].

Floatation of light and heavier than bed solids were explored earlier, and it opened many questions. It was never tried for separation of particles larger than group D. So, this potential needs to be explored experimentally.

We designed a bench scale unit meeting the capacity of fan availability at Allan Equipment. The first task was to study the basic characteristics of the fluidized bed, such as the distribution characteristics, bed pressure drops vs the fluidization characteristics. After establishing this base line date, we started experimenting with a mixture of rock and potato of similar sizes, to test if a fluidized bed of group B fine particles could indeed separate such large particles.

After initial encouraging results, we set out in examining how fluidization velocity affects the degree of separation of potato from a mixture of rock and potato.

3.2 BACKGROUND OF FLUIDIZED BED

The concept of fluidization although has been around from the early 1940's, has only been researched in detail over the past few decades and has found its application in many industrial sectors. The very first reported occurrence of fluidization took place in 1920, when researcher Fritz Winkler had introduced a fluid at the bottom of a crucible containing coke particles, resulting the particles to be lifted by the drag of the fluid medium making the crucible appear like a boiling liquid [21].

Fluidized beds are used widely in boiler industry because of their many advantages in the combustion processes. The use of fluidized beds promotes high heat and mass transfer rate, uniform heat distribution. Early fluidized beds built were primarily used for catalytic cracking in the chemical sector. Later it was actively used for burning coal due to its enhanced heat distribution and insensitivity towards fuel quality. The second

generation of fluidization that took over was the circulating fluidized bed and lead to the use of these systems in coal combustion systems and steam generation.

3.2.1 Application of fluidized beds

In addition to the usage of fluidized bed in boilers, they find use in other sectors of the industry as well. The fluidized beds are used in food processing sector and are used in applications like freezing, drying, puffing, spray drying and blanching. The freezing of veggies and other berries are carried out with the help of fluidized beds. Puffing is the process in which the food products like potato, carrots and beans are buffed up varying the temperature range of the fluidized bed. In Agro products drying was a popular application of fluidized beds. Solar assisted bed dryer, Microwave assisted bed dryer and Heat pump assisted bed driers are also used [22]. These systems function effectively than other means of drying because of their easy adaptability to various drying processes. To quickly freeze the food sample, fluidized beds have been used and proved to be very effective. [23]

An advanced and complex use of fluidized bed in waste waster treatment was put out in this article by Bello et al [24]. Employing a fluidized bed in wastewater treatment can be a cost-effective method, supporting advanced oxidation processing and biological treatment of water. Fluidized beds have been established to function as good medium for wastewater treatment by previous researchers in oxidation processes [25] and denitrification [26].

Fluidized beds could have potential use for separation of binary particles. Zaltzman [7], explored the separation of flower bulbs from clods and stones, and found out that the effectiveness of the fluidized bed separator was in the high ranges of 90-95%. Detailed exploration of separation of binary particles like potato and rocks is awaited.

3.2.2 Fluidization

The research motive in using fluidization is to understand the characteristics of potato and rock when they are introduced into a fluidized bed of fine particles and explore if this process can be used to separate potato from rocks. The test was carried out in a fluidized bed with sand as the bed material. The characterization study was carried out to understand, at certain fluidization velocities the distribution of rocks and potatoes inside the bed. This floating and sinking characteristics of binary particles (Potato and

Rock) is compared by making use of potatoes of the same densities and similarly rocks of the same density. By varying the density of the bed, achieved by changes in velocity of air supply, the study is conducted.

3.2.3 Flow regimes

A fluidized bed may be operated under several regimes. The flow regimes of fluidization are explained in short as follows:

- **Fixed Bed**: This is the stage in which the bed is in its initial condition when the air supply from below is minimal.
- **Bubbling Regime**: In this stage, as the superficial gas velocity increases the bubbling starts to take place. This is the initial stage of fluidization.
- **Slugging and Turbulent Regime**: These stages denote the points at which the bed material begins to break down and bubbling occurs vigorously.
- **Fast and Pneumatic Conveying Regime**: When the particles are transported outside the bed after it reaches a certain transport velocity (U_{th}), this fluidization regime state is achieved.

A schematic of the transition of fluidization regimes for increasing gas velocity in shown in Figure 35 [20]

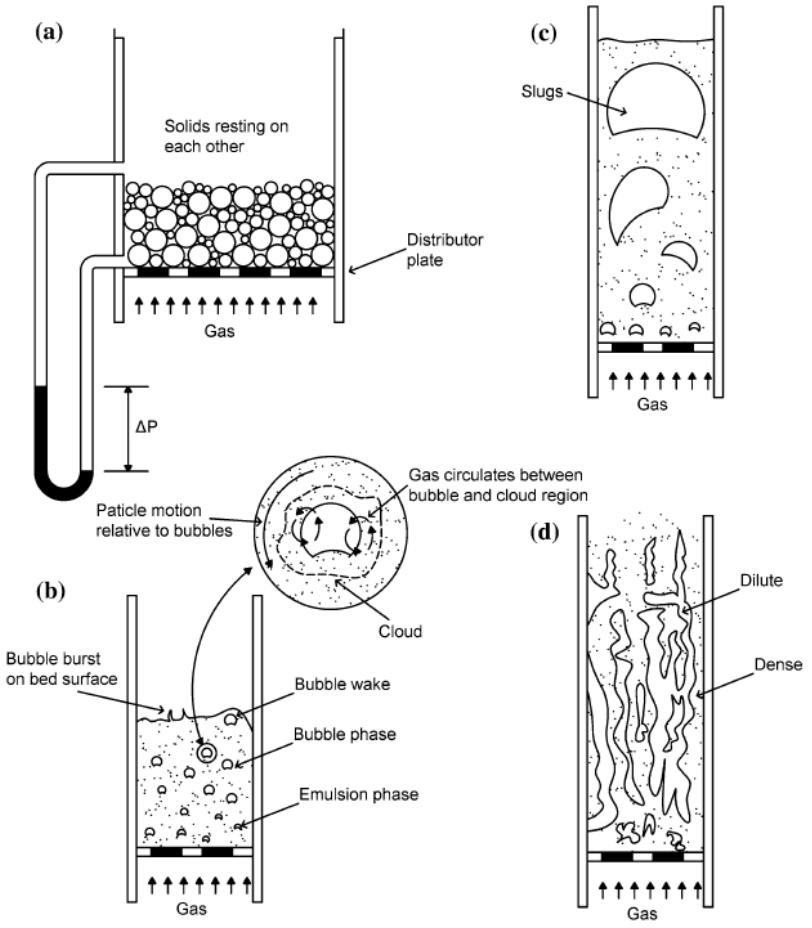

Figure 35**. a)** Fixed bed **b)** Bubbling bed **c)** Slug bed **d)** Turbulent Bed [20]

In a gas solid fluidized bed, it has been established by previous researches that the flow transitions to a fluidized bed from a fixed bed state upon achieving a minimum fluidization velocity (U_{mf}). In a fixed bed state, the air moving across the particles does not have the required velocity to lift or move the bed materials. The system involving gas-solid fluidization is effectively dependant on the gas and solid interaction. With a steady increase in gas flow or superficial gas velocity (U_g), different fluidization regimes occur. When a certain superficial gas velocity is achieved bubbles start to form and rise in the packed bed causing mixing of the particles. The bubbles start to occur when the minimum bubbling velocity (U_{mb}) is achieved. Slugging appears in cases where the bed height to diameter ratio is above 2. The bubbles in this regime are very large and are called slugs. For fine particles, the factors such as minimum bubbling velocity (U_{mb}) and minimum slugging velocity (U_{ms}) play a major part in determining the flow regime. A turbulent regime occurs when the superficial gas velocity reaches a maximum to critical velocity (U_c). When the slugs reach this velocity, the bubbles tend to break and stop growing. This breakage of bubbles cause turbulence in the fluidized

bed system. When this condition is achieved entrainment of particles begin to occur in the bed of a fixed diameter (D). When the superficial gas velocity reaches the transport gas velocity (U_{th}), a state is fast fluidization is reached. A further increase in the transport velocity causes the bed material to be thrown out of the bed, leading to a dilute phase. This final stage of the flow regime, wherein the particles are thrown out of the bed is the pneumatic conveying regime [27].

A flow chart depicting the transition of regimes is shown in Figure 36, for an increasing gas velocity and the corresponding bubble diameter (D_b) affecting it in the process.

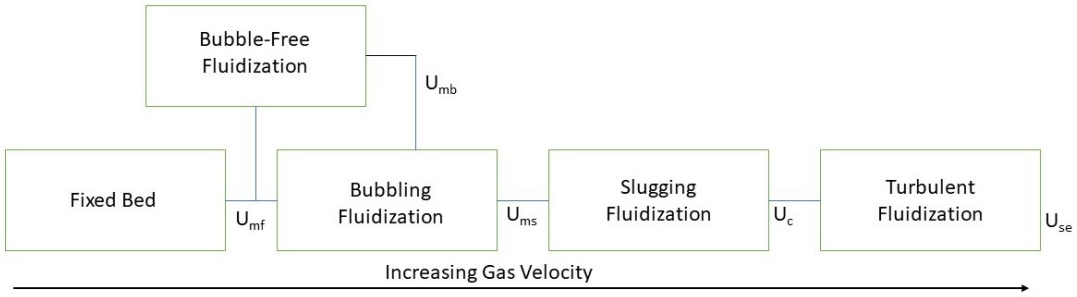

Figure 36. Transition of flow regimes [28]

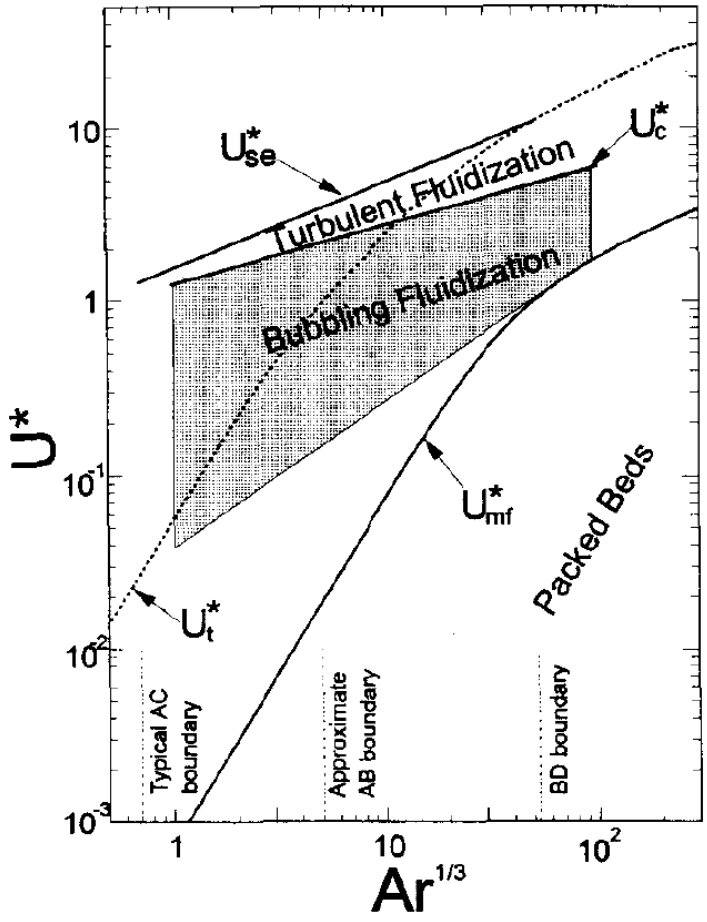

Figure 37. Flow regime map [28]

Particles are classified based on their sizes and differentiated as Group A, B, C & D Geldart particles.

- **Group C** particles are cohesive in nature and are very fine particles. Group C particles are difficult to fluidize because of their cohesive nature.
- **Group A** particles are aeratable and have low particle density and are relatively easy to fluidize under controlled bubbling conditions.
- **Group B** particles are almost sand-like and have a particle size 40μm to 150μm. These particles fluidize easily and vigorously.
- **Group D** particles are the large density particles. These particles are generally not suited for fluidization applications since they act irrationally upon fluidization.

In the present research potato and rocks particles are to be separated, and they fall under either Group D or beyond that range. None reported to have fluidized particles as large as these particles which are typically in the range of 50 -100 mm. So, this rules out the possibility of using bubbling fluidized bed for this range.

To avoid this, we decide to use a bed of finer particles sand, that belong to Geldart B. Initial experiment is carried out with large size of about 750 microns. But it gave minimum fluidization velocity much too high for the capacity of the available fan to handle. So, for separation we used finer size of sand of mean size of 0.55 mm. This size of sand is used to make sure that there is uniformity in fluidization.

The Geldart groups can be defined by their Archimedes number and previous researchers have found a correlation to predict the minimum fluidization velocity for different Geldart particles. In a journal article published by Rabinovich and Kalman [29] the conditions for the range of the Reynolds number for the different Geldart particles have been listed.

For Geldart A particles (1<Ar<80):

$$Re_{mf} = 0.0008Ar \qquad \text{Eqn. [10]}$$

For Geldart B particles (80<Ar<30000):

$$Re_{mf} = 0.000955Ar^{0.96} \qquad \text{Eqn. [11]}$$

For Geldart D Particles (Ar>30000):

$$Re_{mf} = 0.059Ar^{0.56} \qquad \text{Eqn. [12]}$$

3.3. FLUIDIZED BED DESIGN

A Fluidized bed was designed and built at Allan Equipment to carry out the study. This design was constrained by the availability of source of air flow, which could only come from a spare centrifugal fan their shop. This bed was designed with steel as the body material and the sides were made up of glass so that the fluidization can be visible (Figure 42). A porous plate was used as the distributor to make sure that there is even air flow throughout the entire bed width. The design consists of a drain plug at the bottom so that the sand can be drained out manually.

The fluidized bed built of was rectangular in cross section. It is 229 mm x 457 mm in cross section and 952 mm high. The porous plate is made up of Ultra High

Molecular Weight Polyethylene hydrophobic sheet, with a porosity of 70 microns. Opening. The 70 microns porous sheet is chosen to make sure that there is no leak of sand from below. This plate is mounted at 304 mm from the bottom. Below the porous plate is an air chamber which has an opening at the side with a diameter of 150 mm for the fan duct to be connected. Taps were made on the sides of the bed to measure the pressure difference in the fluidized bed.

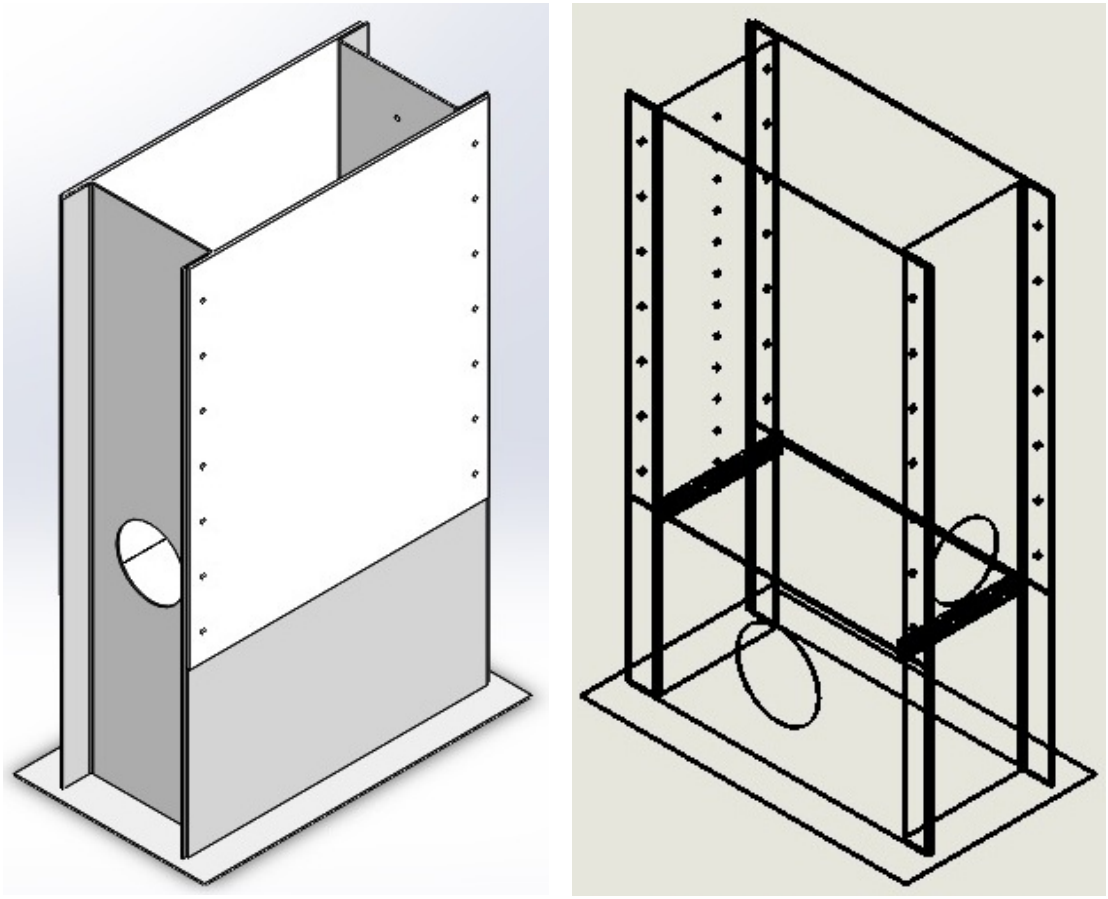

Figure 38. Isometric views of the Fluidizing chamber

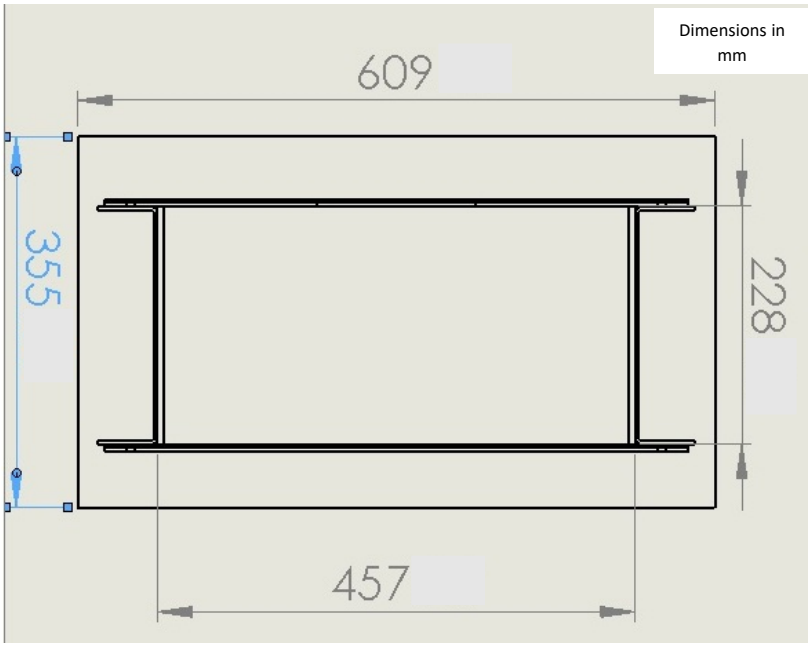

Figure 39. Top View of the Fluidizing chamber

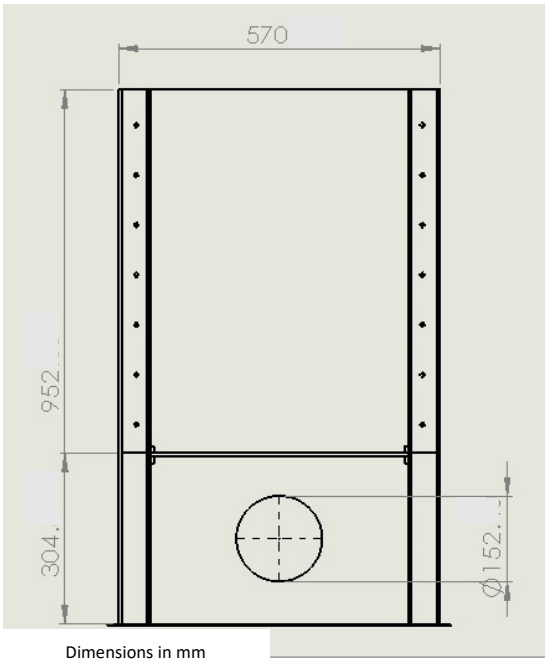

Figure 40. Front View of the Fluidizing chamber

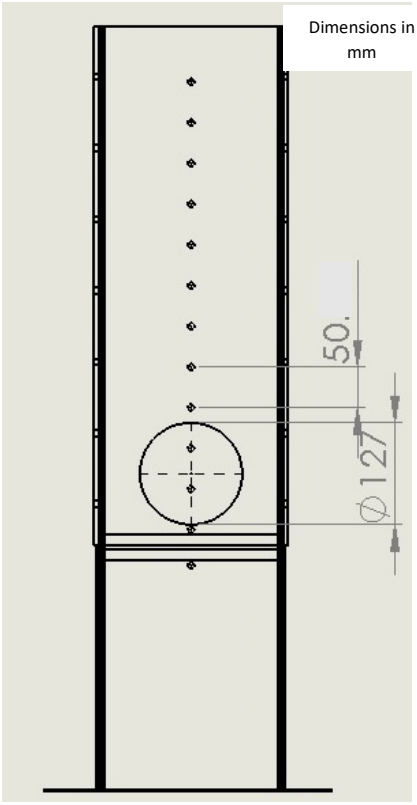

Figure 41. Side view of the fluidizing chamber

Figure 42 a) Photograph of the fan of the fluidized with inlet flow measurement duct

Figure 42.b) Photograph of the fluidized bed built

3.4. DESIGN VALIDATION

Design of the bubbling fluidized bed was constrained as mentioned earlier. Additionally, it was important to verify if the fluidized bed built conforms to classical bubbling fluidized bed characteristics. Following experiments were performed for verification of this design.

3.4.1 Pressure difference across the fluidized bed

The test was carried out with the bed filled initially with 9.7 kg of sand filtered in the range of mean diameter 0.75mm. The pressure difference was measured with the help of a digital manometer. The tubes were connected to a point right above the porous plate and above the sand. This pressure difference measured, helped in calculating the bed pressure difference. It allowed plotting a graph between the velocity and pressure

difference. The flow rate was gradually increased, and the pressure difference was measured as shown in Table 17. The variation in flow rate was achieved by increasing the load of the fan and measuring the flow rate of air at the inlet, which is attached to a flow meter. This pressure difference versus velocity curve (Figure 43) shows us that after attaining a minimum fluidization velocity the pressure difference across the remains constant even after further increasing the velocity. This shows the minimum fluidization velocity of this sand to be 0.6 m/s which very close to that theoretically calculated and tabulated by Basu (2006, p-457). This experiment confirms that the bed is indeed fluidized. Further increase in the velocity would cause a bubbling. If one continues to increase velocity the bed may enter slugging or turbulent bed regime, none of which are desirable for the present purpose.

One observes the familiar hysteresis characteristics of large particle fluidized here. While the velocity was gradually increased the bed pressure drop at each velocity is higher than that obtained while the velocity was decreasing. This happens because while gas flows through the interstices of particles in a fixed bed a high resistance in encountered. Once the bed is fluidized the particles rearrange themselves into most comfortable position that offers the least resistance to the gas. Thus, when velocity is decreased back from fluidized to fixed bed condition we note that the resistance in each corresponding velocity is lower than that obtained earlier.

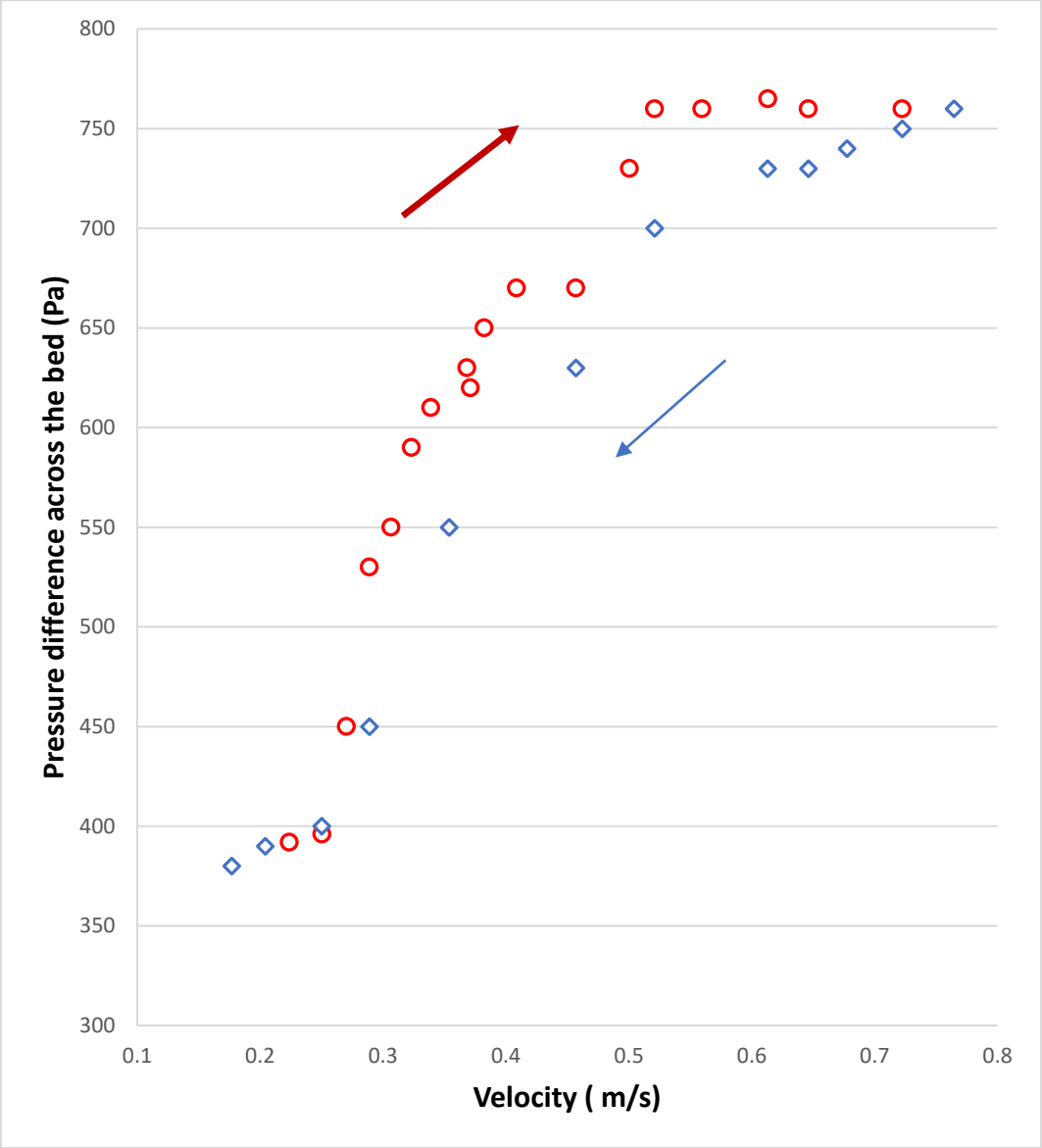

Figure 43.Pressure difference measured across the bed of 0.75 mm sand particles. Data plotted against both rising and decreasing superficial bed velocities showing hysteresis

Table 17. Measured readings for pressure difference across the fluidized bed

Superficial Velocity (m/s)	Pressure (Pa)
0.22	392
0.25	396
0.27	450
0.28	530
0.30	550
0.32	590
0.33	610
0.37	620
0.36	630
0.38	650
0.40	670
0.45	670
0.50	730
0.52	760
0.55	760
0.61	765
0.64	760
0.72	760
0.76	760
0.72	750
0.67	740
0.64	730
0.61	730
0.52	700
0.45	630
0.35	550
0.28	450
0.25	400
0.20	390
0.17	380

3.4.2 Characterization of the distributor plate

The fluidized bed used a 70-micron porous plate as its distributor plate whose function is to support bed materials and uniformly distribute the air entering the fluidized bed. The pressure difference across the distributor plate was measured by connecting the manometer at point's right above and below the porous plate. This test was carried out in the chamber without the bed material

Pressure drop across distributor without bed material

The test was carried out in the chamber without any bed material present in it. By varying the flow rate of the air entering the fan, the pressure difference across the bed was measured. (Table 18)

Table 18. Pressure difference across the porous plate without sand

Superficial Velocity (m/s)	**Pressure Drop (Pa)**
0.79	2937.16
0.72	2861.32
0.65	2723.42
0.56	2551.06
0.46	1965.00
0.32	1620.26

Case 2: Chamber with bed material:

As the minimum fluidization velocity of 0.75 mm particle was high we chose to use finer size of sand in the range of 0. 55 mm. The second test was carried out by filling out the chamber with this finer bed material, sand. Calculated minimum fluidization velocity of this sand was 0.21 m/s

The test was carried in a similar way by increasing the flow rate and measuring the pressure difference between the porous plate. (Table 19)

Table 19. Pressure difference across the porous distributor plate with sand filled

Superficial Velocity (m/s)	**Pressure Drop across distributor (Pa)**
0.500	1076
0.456	1010
0.408	990
0.382	930
0.353	900
0.323	880
0.288	820
0.288	820
0.323	870
0.353	880
0.382	920
0.408	950
0.456	990
0.500	1060

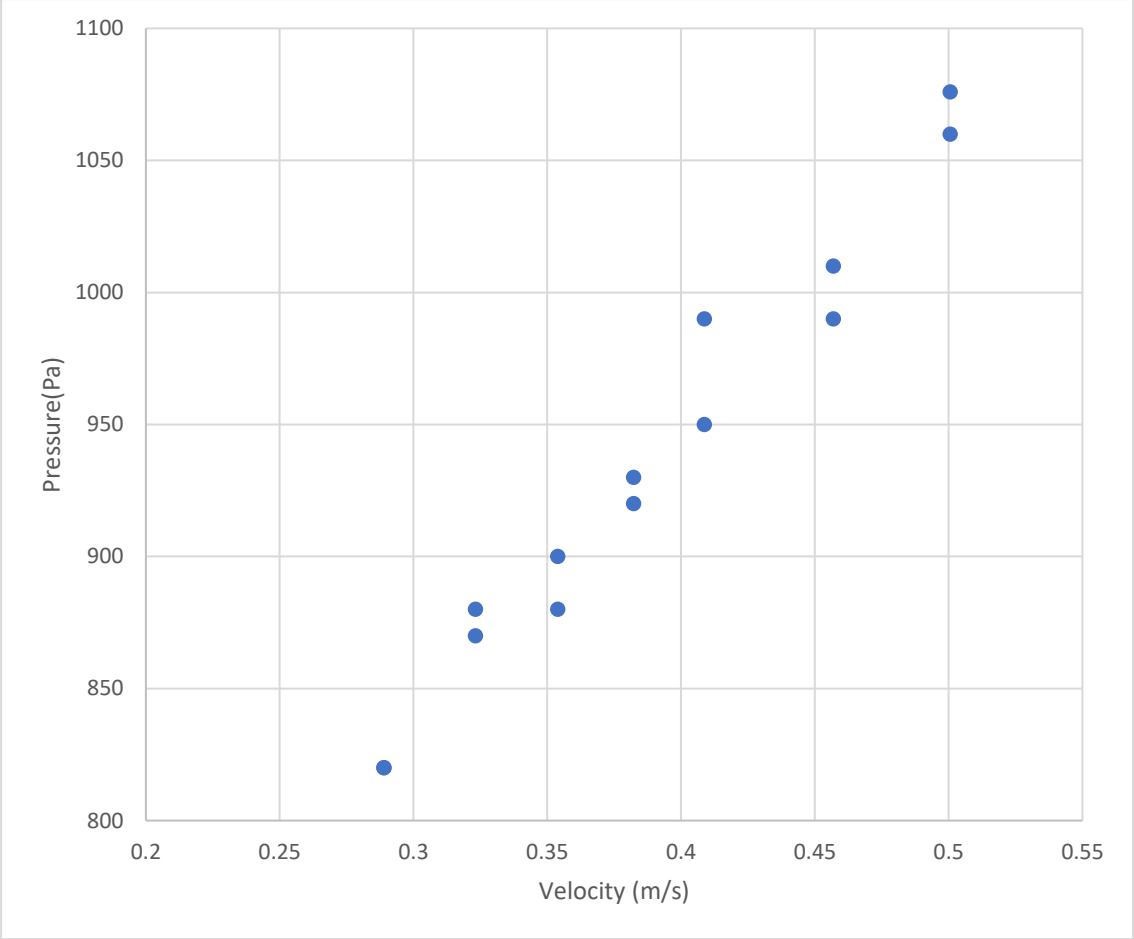

Figure 44. Pressure difference across the porous plate vs Velocity

3.4.3 Variation of bed height with change in velocity

When air is passed through a packed bed, the bed expands. This is based on the various fluidization regimes as explained in section 3.2.3

In order to make sure that the bed expansion is within an acceptable range, a test was carried out to find out the variation in bed height with respect to velocity. Peer reviewed literatures have shown many papers which shows relationship between the bed hydrodynamics and bed height. These papers show various fluidized bed regimes and the effect of fluidization velocity on the increase in bed height as well. In the work carried out by Sau et al [30], the study was conducted on taper/conical beds which showed that the tapered angle affected the fluidization velocity, but the bed height does not change much with change in the fluidization velocity. It is primarily due to the conical shape of the bed.

Gunn and Hilal [31], conducted experiments on solid-gas fluidized beds in a cylindrical bed. The bed material was glass beads of different sizes. They studied how the bed heights varied with the change in fluidization velocity. Shaul et al [32] showed that for all Geldart particles for the same Archimedes number the H/D ratio remains the same. The group B particles when increasing the superficial gas velocity from bubbling to slugging, in case of higher bed heights behave as group D particles. For spherical and

Table 20. Velocity and change in bed height for 0.55 mm finer sand

Flow rate at the fan suction section (m^3/s)	Fluidization Velocity(m/s)	Expanded Bed Height (mm)
0.030	0.289	319
0.034	0.323	323
0.037	0.354	331
0.040	0.382	336
0.043	0.409	343
0.048	0.457	349
0.052	0.500	355

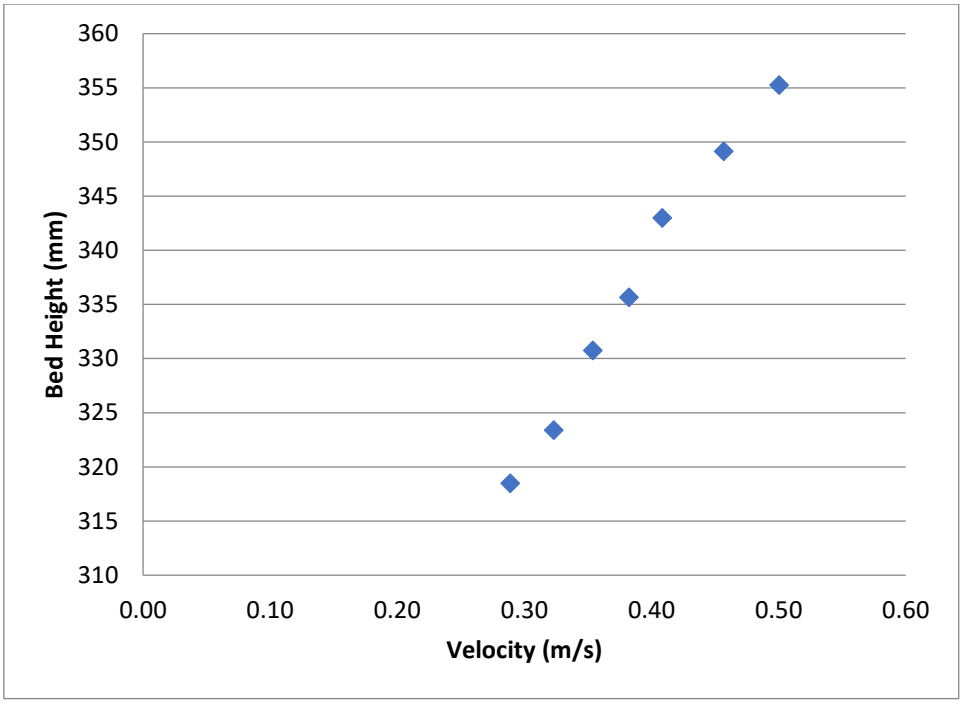

Figure 45. Velocity vs expanded bed height for 0.55 mm sand fluidized bed

3.5 FLUIDIZATION OF ROCK AND POTATO

The analysis of sinking and floating of the potatoes and the rocks in the sand chamber was carried out. The fluidization of a material in the bed is dependent on various factors such shape, size, density and fluidization velocity. To understand the effects of density and velocity on the potatoes/rocks, the layer test was carried out.

3.5.1 Density measurements for objects under study

The potatoes and rocks that are collected by the harvester are of different sizes and shapes. Hence potatoes and rocks of different sizes were collected, and the densities were found out for these samples. The samples that were collected were subjected to manual measurement of density using a weighing balance scale, beaker, and water. The mass of the object is weighed, and the same object is immersed in a beaker filled with water. Since the density of water is 1000 kg/m^3, the mass (of Potato/Rock) obtained after immersing the object in water directly provides the volume of the object. Dividing the mass of the object by the volume obtained through the experiment provides us with the density of the object which is under study.

Figure 46. Potatoes and rocks sorted based on size

Table 21. Density of the sample of potatoes collected

Potato #	Mass(g)	Volume (cm^3)	Density (kg/m^3)	Spherical Diameter (mm)
1	69	62	1112.90	48.34
2	80	73	1095.89	51.02
3	94	85	1105.88	53.64
4	73	67	1089.55	49.59
5	65	57	1140.35	47.02
6	101	92	1097.83	55.06
7	75	67	1119.40	49.59
8	106	97	1092.78	56.03
9	118	109	1082.57	58.23
10	107	98	1091.84	56.22
11	88	77	1142.86	51.92
12	84	74	1135.14	51.24
13	123	112	1098.21	58.76
14	105	95	1105.26	55.65
			Average	**53.02**

Table 22. Density of the sample of rocks collected

Rock	Mass(g)	Volume (cm^3)	Density (kg/m^3)	Spherical Diameter (mm)
1	147	70	2100.00	50.31
2	170	84	2023.81	53.43
3	147	73	2013.70	51.02
4	139	68	2044.12	49.83
5	140	69	2028.99	50.08
6	154	75	2053.33	51.47
7	129	64	2015.63	48.85
8	123	60	2050.00	47.82
9	140	68	2058.82	49.83
10	150	74	2027.03	51.24
			Average	**50.39**

3.5.2 Layer tests

In order to find out axial distribution of potatoes and rocks inside the sand chamber, a characterization study was carried out. This experiment is most efficient when done using an X-ray machine, to find out the exact position of the object inside the sand chamber without causing any change in position after the fluidization is stopped. This system was not economically viable and hence alternate means of carrying out the study was required.

The sectioning of the bed into individual layers and manual removal of the sand from the sand chamber were done in order to carry out the quantitative study. This manual separation although does not provide very high accuracy, is the best viable option to carry out the study.

The study involved the fluidization of the sand chamber and dropping down potatoes and rocks of segregated samples from the top. The sand chamber was fluidized at various superficial gas velocities, and it was allowed to run for at least two minutes. By adjusting the load of the fan and therefore the delivered flow rate, bubbling in the bed is achieved. Then the flow rate is kept constant for a time period of two minutes after which the fan is stopped abruptly. After the fluidizing chamber is completely shut down, the sand is removed from the layers 5-1. The number of rocks and potatoes in each layer is noted.

The same experiment is carried out by changing the flow rate in steady increments. The test is stopped at a point where the separation is fully achieved, after which further increase in velocity would change the bed's flow regime.

The sand chamber is divided into 5 layers, every 63.5 mm in length from below. This is shown in Figure 47.

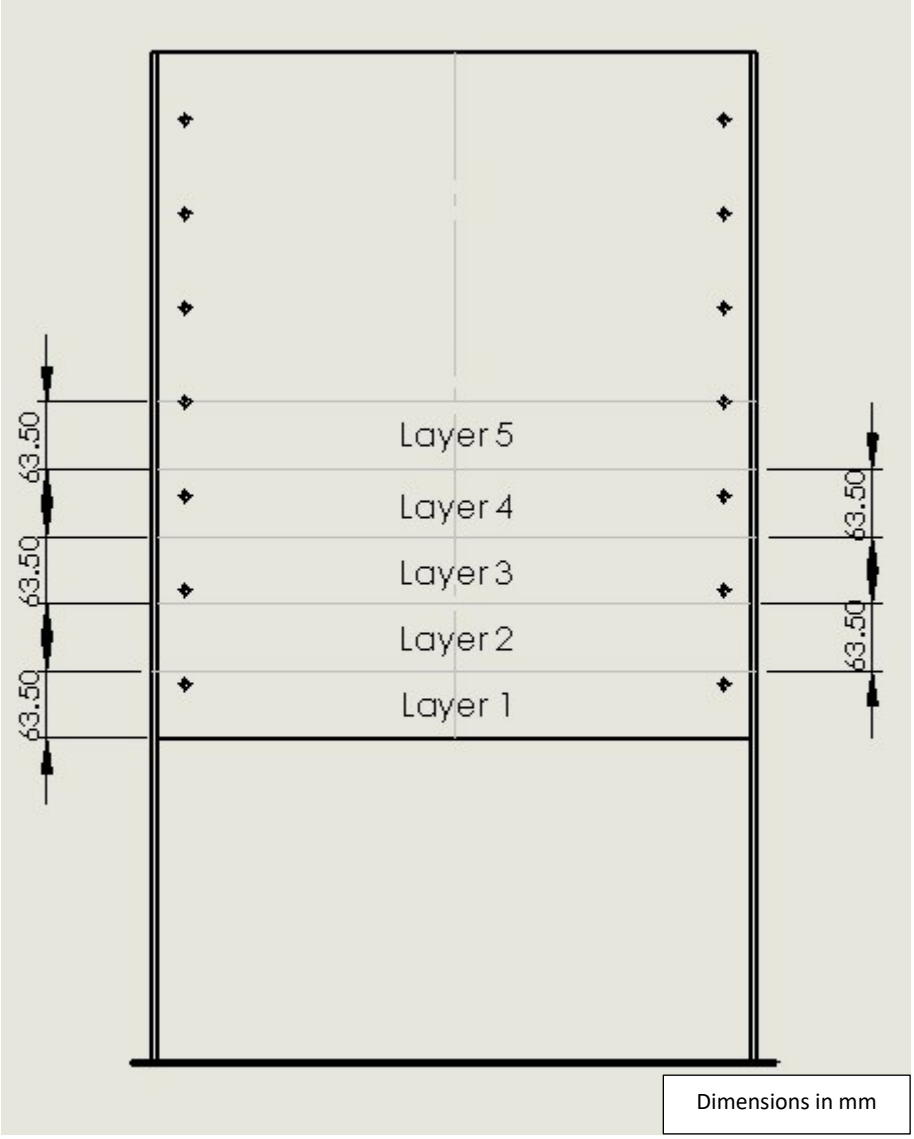

Figure 47. Sectioning of the sand chamber into layers

3.5.3 Size distribution of sand in the fluidized bed

In this study, we have the sand sieved based on the desired size. The size of sand plays an important part in determining the fluidizing velocity. The sand that was collected was construction sand, which was sieved in narrow range, to achieve the desired particle size.

Two sizes of sand were used with narrow size range. The first one had a mean size of 0.75 mm while the second one was 0.55 mm. The first type was used to measure minimum fluidization curve while the second one was used for separation of rock and potato

3.6 RESULTS & DISCUSSION

The distribution of rock and potato in different horizontal layers in the bubbling fluidized bed was carried out in the experimental setup, explained in the above sections. In the tests carried out, it was found that the potatoes at a fluidization velocity, float on the top but the rocks stay at the bottom. Above this particular velocity the tendency of jetsam (The particles that are at the bottom of the bed) and flotsam (The particles that are up on the surface of the bed) do not change. Potatoes and rocks of different sizes and density were use in the process of this experiment. Table 23 shows the air flow rate and the particle population in different layers of the fluidized bed.

Table 23. Layer test for fluidized bed. Layer tests carried out for Potato size 53 mm, Rock size: 50mm

	Distance from the top to bottom in mm		Top		Middle		Bottom
			254-317.5	190.5-254	127-190.5	63.5-127	0-63.5
	Average Distance		285.75	222.25	158.75	95.25	31.75
Velocity		Layer	5	4	3	2	1
(m/s)							
0.28		Potato	14	0	0	0	0
		Rock	0	3	2	1	4
0.32		Potato	14	0	0	0	0
		Rock	0	3	0	1	6
0.35		Potato	14	0	0	0	0
		Rock	0	2	0	0	6
0.38		Potato	14	0	0	0	0
		Rock	0	0	0	0	10
0.40		Potato	14	0	0	0	0
		Rock	0	0	0	0	10
0.45		Potato	14	0	0	0	0
		Rock	0	0	0	0	10
0.50		Potato	14	0	0	0	0
		Rock	0	0	0	0	10

The Figure 48 shows the layer test results in which the potato and rock are distributed along the bed height at different fluidization velocities. At the lowest velocity of 0.28 m/s, the rocks are distributed along different layers of the bed. But at the maximum velocity rocks are all at the bottom of the bed but the potatoes float on the surface. At any given velocity, the potatoes stay on the top suggesting efficient separation.

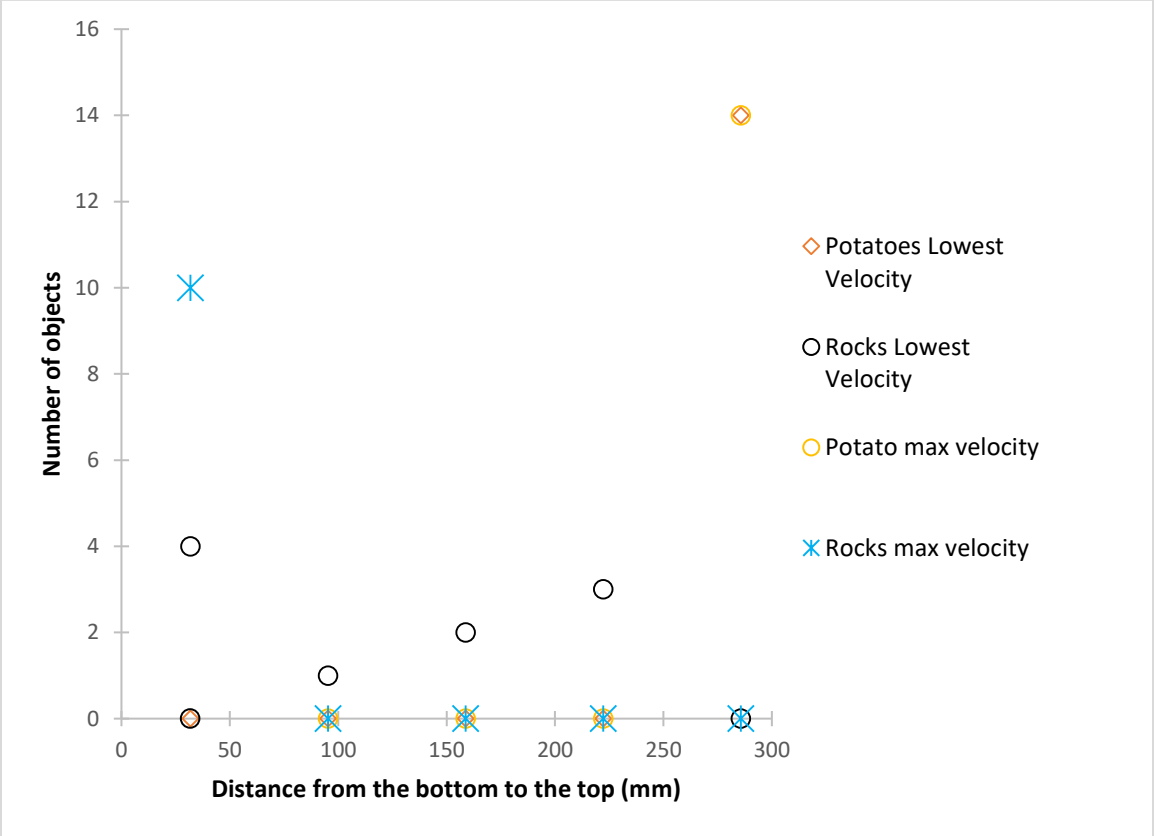

Figure 48. Layer test results showing segregated binary components (Potato & Rock)

3.7 SUB-CONCLUSIONS

This part of the research was to develop a new type of separator using fluidized bed principles. Following conclusions were derived from this work:

1. It is possible to separate particles as large as 50-55 mm in a fluidized bed of particles as fine as 0.55 mm
2. The degree of separation of rock and potato particles in such fluidized bed depends on the fluidization velocity
3. For the bubbling fluidized bed of 0.75 mm sand optimum fluidization velocity of separating 52 mm potato from 50 mm rock was 0.38 m/s.

Chapter 4: CONCLUSION AND RECOMMENDATION

This chapter presents the overall conclusion of this work and recommendations for future work.

4.1 CONCLUSIONS

1. This work succeeded in assisting Alan Equipment company of PEI in improving their current design of potato-rock separator.

2. Non-uniform airflow distribution above the plenum was the main cause of inefficient separation.

3. CFD simulation, validated by later experiments, showed that flow uniformity could be achieved by relocating the fan in front of the plenum entry and by placing a perforated plate at the plenum exit.

4. Additional experimental work showed that it is possible to achieve specific air distribution that AE wanted, by rearranging the size and distribution of holes in the perforated plate. Layout IV and Case 9 (Section 2.3.9) was best for this design.

5. Fluidized bed of sand was used for separation of wide range of solids from very fine to very large particles.

6. For improved design bubbling fluidized bed of small (~0.55 mm) sized sand can be used to separate much larger size (~50 mm) potato and rock particles.

7. Separation is a function of fluidization velocity in the bed.

8. For the given combination of bed material and potato-rock optimum fluidization velocity was 0.38 m/s.

4.2 RECOMMENDATION FOR FUTURE WORK

A major challenge for this research was its carrying out in an industry with limited R&D resource and limited availability of time and funds. Experiments on the full scale commercial unit, further restricted the flexibility of research. So, extensive experiments

varying all relevant parameters over their full range, as expected in an academic research could not be accomplished. The work had to be limited to whatever facility and time available at the plant of Allan Equipment could provide us with. For detailed exploration following work are suggested:

1. For Chapter 2, more comprehensive work on CFD could be carried out that could handle variation of hole size over the large plate area
2. AE need to procure a centrifugal fan of higher head such that it can overcome the additional pressure drop of perforated plate
3. A low resistance flowmeter needs to be procured and installed for more comprehensive investigation of flow parameters.
4. For Chapter 3, work could be carried out over a wider range of bed particle size
5. Segregation of other sizes of rock and potato could be studied
6. Separation of rock and potato of wide size distribution needs to be checked
7. Scale up parameters need to be developed and tested in commercial size.

REFERENCES

[1] H. Holmes, "Scottish agricultural implement makers," 26 April 2015. [Online]. Available: http://blog.scottishagriculturalimplementmakers.co.uk/?p=238. [Accessed 01 06 2019].

[2] S. E. C. LLC, "Harvester 3 Row Air," [Online]. Available: https://www.spudnik.com/equipmentDetail/equipmentDetail.php. [Accessed 02 06 2019].

[3] K. Kalverkamp, F. Dettmer and C. Döhmann, "Separation system for a potato harvesting machine or a preparation machine". Patent WO2014026766A3, 30 May 2014.

[4] N. D. Leighton and G. O. Leighton, "Air suction potato conveyor harvesting machine". United States of America Patent US3227276A, 04 January 1966.

[5] D. E. Systems, "Milestones-Equipment," [Online]. Available: http://www.milestone-equipment.com/debris-elimination-systems. [Accessed 02 06 2019].

[6] C. HOPPER, "Harriston-Mayo," [Online]. Available: http://www.harriston-mayo.com/harriston/clod-hopper.php. [Accessed 02 06 2019].

[7] A. Zaltzman, R. Feller, A. Mizrach and Schmilovitch, "Separating Potatoes from Clods and Stones in a Fluidized Bed Medium," *American Society of Agricultural and Biological Engineers,* vol. 26, no. 4, 1983.

[8] P. Moin and J. Kim, "Tackling Turbulence with Supercomputers," *Scientific American - SCI AMER,* vol. 276, pp. 62-68, 1997.

[9] B. Xia and D.-W. Sun, "Applications of computational fluid dynamics (cfd) in the food industry: a review," *Computers and Electronics in Agriculture,* vol. 34, no. 1-3, pp. 5-24, 2002.

[10] S.-E. Kim and F. Boysan, "Application of CFD to environmental flows," *Journal of Wind Engineering and Industrial Aerodynamics,* vol. 81, pp. 145-158, 1999.

[11] I. Celik, "RANS/LES/DES/DNS: The Future Prospects of Turbulence Modeling," *Journal of Fluids Engineering,* vol. 127, no. 5, pp. 829-830, 2003.

[12] C. Sharad and K. Santosh, "Performance Analysis of Backward Curved Centrifugal Fan in Heating Ventilation and Air Conditioning," *International Journal of Science and Research,* vol. 2, no. 6, pp. 170-172, 2013.

[13] N. Ashton and A. Revell, "Comparison of RANS and DES Methods for the DrivAer Automotive Body," in *SAE Technical Paper*, Detroit, 2015.

[14] I. Currie, Fundamental Mechanics of Fluids, New York: Marcel Dekker,Inc, 1993.

[15] A. Kayne, "Computational Fluid Dynamics (CFD) Modeling of Mixed Convection Flows in Building Enclosures," *All Theses and Dissertations (ETDs),* p. 740, 2012.

[16] A. E. Byl, "Characterization of airflow through an air handling unit using computational fluid dynamics," *Theses and Dissertations at Montana State University (MSU),* 2015.

[17] L. Palanti, D. Pampaloni, A. Andreini and B. Facchini, "Numerical simulation of a swirl stabilized methane-air flame with an automatic meshing CFD solver," *Energy Procedia,* vol. 148, pp. 376-383, 2018.

[18] J. Zahradník, G. Kuncová and M. Fialová, "The effect of surface active additives on bubble coalescence and gas holdup in viscous aerated batches," *Chemical Engineering Science,* vol. 54, no. 13-14, pp. 2401-2408, 1999.

[19] M. Ruzicka, J. Drahoš, J. Zahradník and N. Thomas, "Structure of gas pressure signal at two-orifice bubbling from a common plenum," *Chemical Engineering Science,* vol. 55, pp. 421-429, 2000.

[20] P. Basu, Circulating Fluidized Bed Boilers, Halifax: Springer International Publishing, 2015.

[21] A. M. Squires, " Fluidized bed combustion and applications," *In J. R. Howard (Ed.),* p. 278, 1983.

[22] R. Sivakumar, R. Saravanan, A. ElayaPerumal and S. Iniyan, "Fluidized bed drying of some agro products – A review," *Renewable and Sustainable Energy Reviews,* vol. 61, pp. 280-301, 2016.

[23] N. Shilton and K. Niranjan, "Fluidization and Its Applications to Food Processing," *Food Structure,* vol. 12, no. 2, 1993.

[24] M. M. Bello, A. A. A. Raman and M. Purushothaman, "Applications of fluidized bed reactors in wastewater treatment – A review of the major design and operational parameters," *Journal of Cleaner Production,* vol. 141, pp. 1492-1514, 2017.

[25] F. Tisa, A. A. A. Raman and W. M. A. W. Daud, "Applicability of fluidized bed reactor in recalcitrant compound degradation through advanced oxidation processes: A review," *Journal of Environmental Management,* vol. 146, pp. 26-275, 2014.

[26] G. Zou, S. Papirio, E. v. Hullebusch and J. Puhakka, "Fluidized-bed denitrification of mining water tolerates high nickel concentrations," *Bioresource Technology,* vol. 179, pp. 284-290, 2015.

[27] D. R. Escudero, "Bed height and material density effects on fluidized bed hydrodynamics," *IOWA STATE UNIVERSITY CAPSTONES, THESES AND DISSERTATIONS,* 2010.

[28] H. BI and J. Grace, "FLOW REGIME DIAGRAMS FOR GAS-SOLID," *International Journal of Multiphase Flow,* vol. 21 , no. 6, pp. 1229-1236, 1995.

[29] E. Rabinovich and H. Kalman, "Flow regime diagram for vertical pneumatic conveying and fluidized bed systems," *Powder Technology,* vol. 207, pp. 119-133, 2011.

[30] D. Sau, M. S and K. Biswal, "Minimum Fluidisation Velocities and Maximum Bed Pressure Drop for Gas-Solid Tapered Fluidized Beds," *The Chemical Engineering Journal,* pp. 151-157, August 2007.

[31] D. Gunn and N. Hilal, "The expansion of gas-fluidised beds in bubbling fluidisation," *Chemical Engineering Science,* vol. 52, no. 16, pp. 2811-2822, 1997.

[32] S. Shaul, E. Rabinovich and K. Haim, "Generalized flow regime diagram of fluidized beds based on the height to bed diameter ratio," *Powder Technology,* vol. 228, pp. 264-271, 2012.

[33] R. Sarker, M. Rahman, N. Love and A. Choudhuri, " Effect of Bed Height, Bed Diameter and Particle Shape on Minimum Fluidization in a Gas-Solid Fluidized Bed," in *50th AIAA Aerospace Sciences Meeting Including the New Horizons Forum and Aerospace Exposition*, 2012.